SPAWAR CST/LLFA-R-EVA-35

MAI 286-U-96-N87

Shallow Water Propagation Comparisons with a SWAC-1 Data Set

31 December, 1996

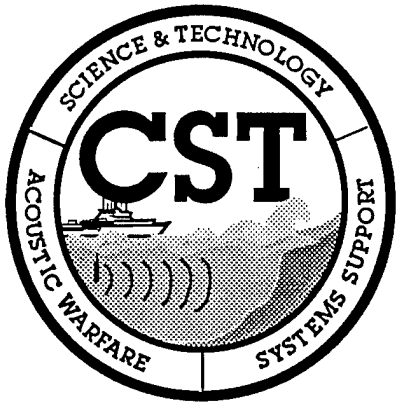

By:

Brian Gardner and Emily McCarthy of MAI,
Jamie Pupek and Robert Gindhart of NAWC

Prepared for:

Space and Naval Warfare Systems Command (PMW-182)
under Johns Hopkins University
Applied Physics Laboratory Subcontract 736676

Abstract

In 1994, during the end of October and the beginning of November, the first Shallow Water Active Classification (SWAC-1) sea trial took place in the Malta Channel region of the Mediterranean. One of the experiments used SUS sources and sonobuoy receivers to measure very shallow propagation effects.

A limited data set is presented with a propagation prediction study using a number of models.

Contents

1. Introduction

In a joint project the Supreme Allied Commander Atlantic Undersea Warfare (SACLANT USW) Research Centre (La Spezia, Italy) and the U.S. Navy conducted the first Shallow Water Active Classification (SWAC-1) sea trial during the period from 18 October through 9 November 1994. This test was conducted in the Malta Channel region of the Mediterranean Sea.

A propagation loss experiment (Event Sierra) was conducted on 3 November (Julian day 307). Data were collected to address important issues in littoral waters and for comparison to propagation model predictions. Event Sierra involved Sound Underwater Signalling Device (SUS) sources and various sonobuoy receivers at three sites (or pods). The sites, designated "A", "B" and "C", are described in Table 1 and the littoral area is depicted in Figures 1 and 2.

Site	Latitude	Longitude	Bottom Depth (m)
A	36.490°N	14.651°E	131
B	36.504°N	14.984°E	49
C	36.226°N	14.983°E	98

Table 1. Sonobuoy drop sites (pods).

To serve as the sound source, explosive SUS were deployed from P3-C aircraft along the radial between location A and B (labeled "AB" in this text), and between C and B (labeled "CB") as shown in Figure 1. The SUS employed were either Mk-82 or Mk-61 (1.8 lbs) types, set for 18.3 m (60 ft)[1]. Sonobuoy recordings were made aboard P3-C aircraft. These analog data were then reduced by the Naval Air Warfare Center (NAWC) at Warminister, PA and processed to obtain range tagged TL values.

A general environmental description of the area can be obtained from the SWAC-1 Quicklook Report **[Ref. 1]**. In the area where the data was collected, nominal wind speeds of 12 knots and wave heights of 3 feet were observed. A northwest to northerly current of about 10 cm/sec was observed near the Event Sierra site.

There were only two *in situ* temperature profiles available for the area, which are shown in Figure 3a. Figure 3b shows the two sound speed profiles

[1]The standard reported detonation depth error is +/- 10 feet.

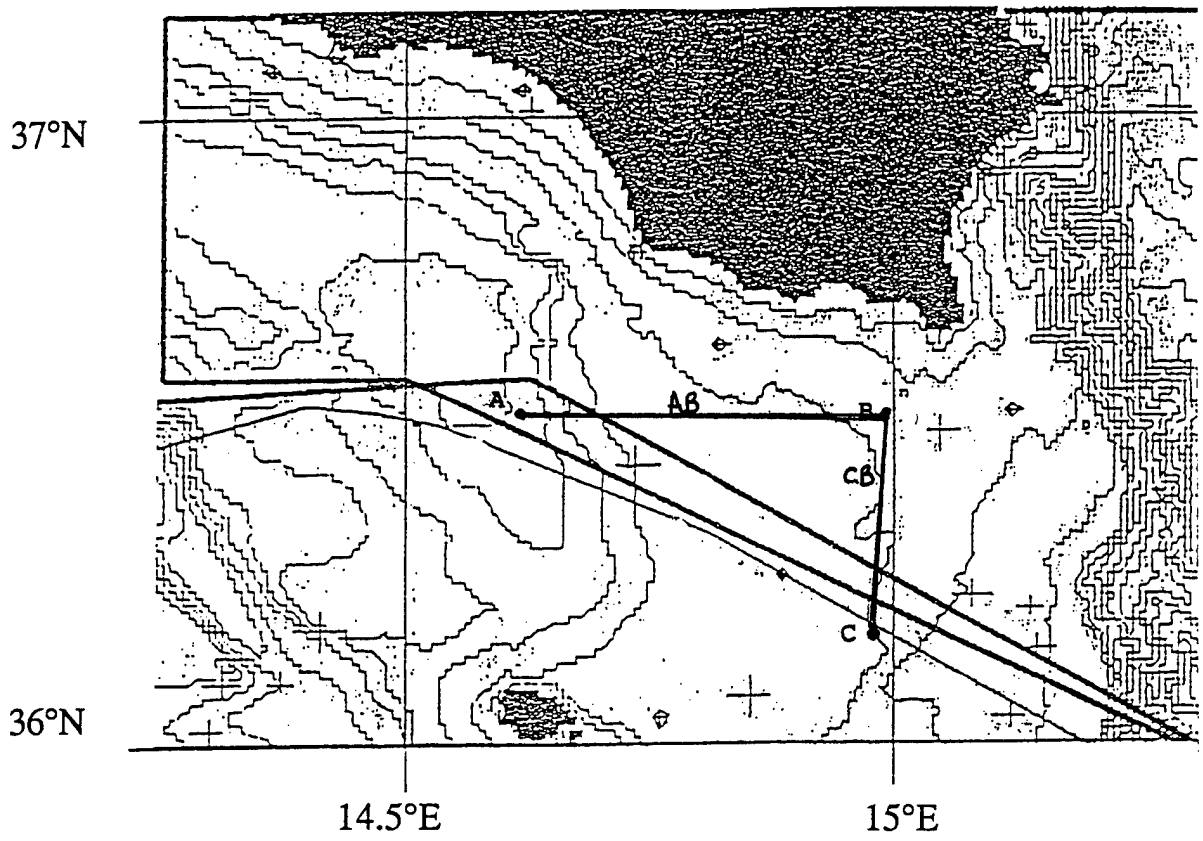

Figure 1. Littoral Malta Channel region.

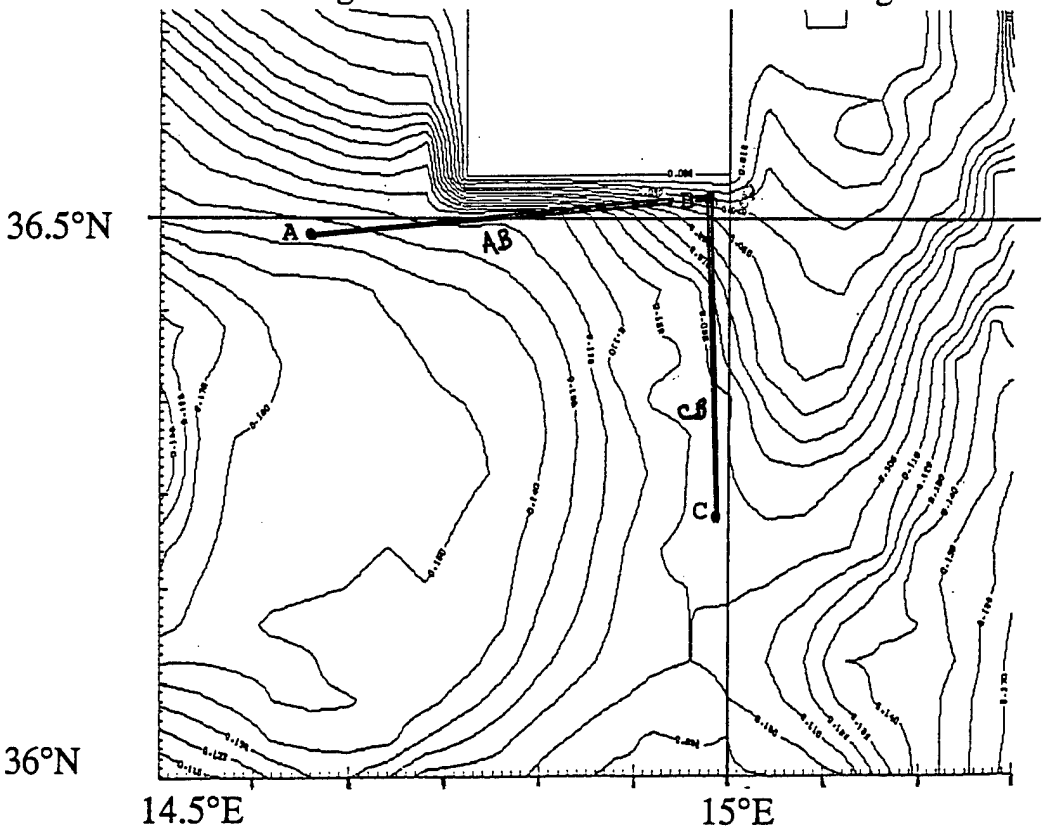

Figure 2. Database representation from the GEM/OAML DBDB-2 database. Bathymetry in 10 m increments. Rectangular patch is an area of no data.

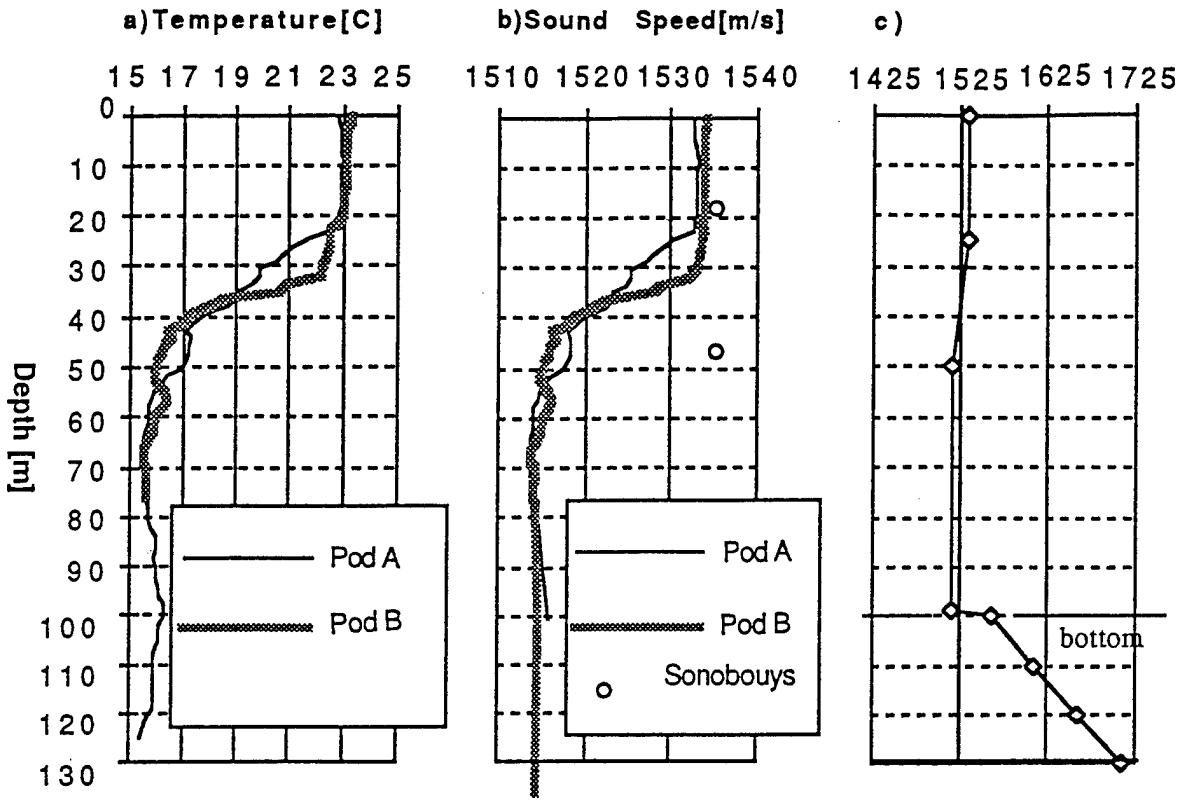

Figure 3. (a) Temperature profiles obtained at sites A and B, and (b) Sound speed profiles (SSPs) calculated from (a). A simplified SSP and sediment sound speed which is used in the environmental analysis is given in (c).

(SSPs) developed from these temperature measurements using a salinity of 37.6 o/oo for A and 38 o/oo for B[2] . The nominal depth of the sonobuoy receivers (18.3 and 47 m, the 47 m receiver was on the bottom) is also indicated in Figure 3-b. To a depth of about 25 m, the sound speed profiles are nearly isospeed. The next layer (roughly 25-50 m) is strongly downward refracting, with a final layer which shows a very gradual slope to the bottom. The shallower sonobuoys were well within the first layer while the bottomed sonobuoy hydrophone lies near the bottom of the second layer. The simple SSP is illustrated in Figure 3c with sound speeds within the sediment layer indicated.

[2] These salinities were obtained from the Composite Area Analysis Model (CAAM) historical data base, GEM **[Ref. 2]**

The shallow bottom is a medium sand with silt and some clay/shells in the AB track, ("Bottom loss may be less than predicted," **[Ref. 1]**) and a silty clay with lesser amounts of sand in the CB track ("Expected bottom loss to be as predicted or can be higher if the clay content extends down several operating frequency wavelengths," **[Ref. 1]**). Since the particular geoacoustic parameters for these two regions are unavailable, a single bottom model was developed for use in this study (Table 2). The sediment is approximately 33 m thick; the sediment sound speed model is illustrated in Figure 3c.

Parameter	Magnitude	Units
Sound Speed Ratio	1.03	--
Initial Gradient	5.0	1/sec
Curvature (Beta)	-0.99	--
Density	1.77	g/cc (ratio)
Attenuation	0.05	dB/m/kHz
Atten Gradient	0.0	dB/m/m/kHz
Sedi Thick(2-way TT)	40.0	ms (2-way)
Shear Sound Speed *	80 * z^0.3	m/s
Shear Attenuation *	1.5	dB/lambda
Porosity *	55.0 %	--
Basement Reflectivity	1.0	--
Sound Speed Ratio *	1.2 to 3.5	--
Density Ratio *	2.0 to 2.7	--
Attenuation *	0.5 to 0.1	dB/lambda
Shear Sound Speed *	600 to 2500	m/s
Shear Atten. *	1.5 to 0.2	dB/lambda

Table 2. Bottom Geoacoustic Parameters.
(Note: These parameters are not used by the propagation prediction models.)

The preceding paragraphs offer a picture of the shallow water environment in which Event Sierra occurred. Sound energy would be expected to undergo numerous interactions with the bottom for the measurement configuration. To present a first look at the anticipated energy paths, the CAAM **[Ref. 2]** raytrace model was run. Ray Traces (+/- 0.5 degrees, in 0.05 degree increments) for an AB[3] and CB shot are given in Figure 4a and 4b. Even over this small source beam width, a large variety of paths are excited. Many more paths would be excited by omni directional sources such as the SUS used here.

The upslope bathymetry of each track is also illustrated in Figure 4. The slope along the sound path causes ever steeper angles of the rays after each interaction with the bottom, so that in fact the angle becomes so steep that sound is prevented from going shallower. The slopes are approximately 0.6 degrees and 0.3 degrees for AB and CB tracks, respectively, and result in a 50% change in the water depth from the source location. The severe down slope extends for approximately 5 nm in the direction of A and 7 nm in the direction of C from point B.

2. Data Analysis

During the Sierra event there were eight sonobuoys (of various attenuations and depths) and one AXBT deployed at each pod. Due to the required attenuation needed (so buoys were not saturated), sonobuoy malfunctions and high Radio Frequency Interference (RFI) conditions, only three buoys from pod B are presented here: one 80 dB and one 40 dB attenuated at 60 ft, and one 80 dB attenuated at 400 ft. A total of 48 SUS (60 ft) were dropped during the test. They were deployed along the AB and BC radials at 1 nautical mile increments with the remainder dropped at each pod for monostatic reverberation data collection.

A SUS signal is unique. It is of such short duration a steady state condition never develops **[Ref. 3].** The exact depth of explosion and the exact signal characteristics (level and spectrum) are not known to the same degree as these parameters are known for pulsed sources.

The bubble pulse for SUS of this weight detonated at 60 feet is 10 Hz **[Ref. 4]**. For this shallow depth, source level information below 50 Hz is not given in

[3] The CAAM database used for modeling lacks information for the region just north of the 36'30" latitude line as evidenced by the rectangular zero depth area in Figure 2. B was placed on the 36'30" line rather than the 36'30.2" position in this and all subsequent modelling runs.

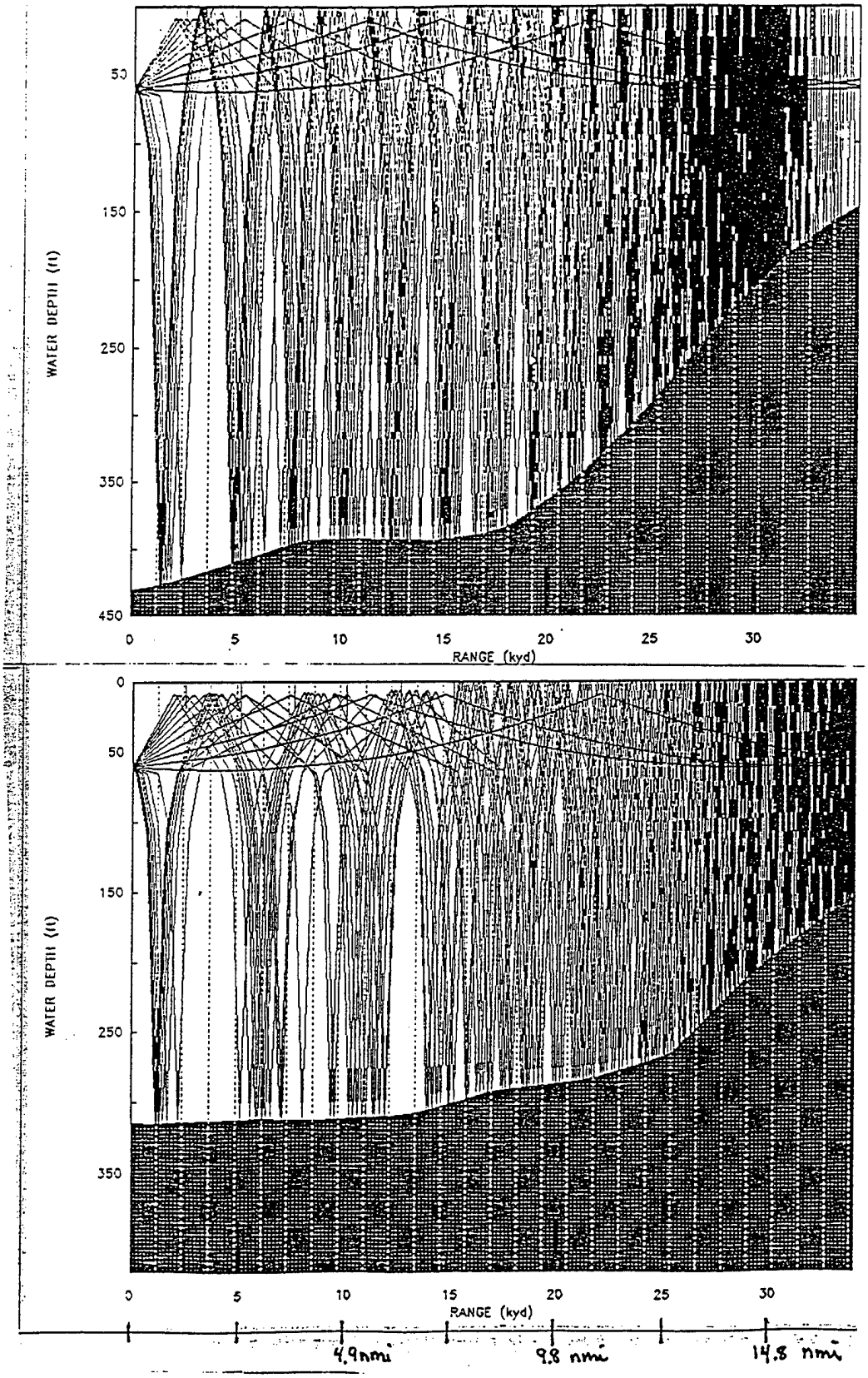

Figure 4. Ray traces produced for each 0.05 degree ray from -0.5 to 0.5 degrees for a). the radial from AB, and b). the CB propagation paths.

the reference. The dotted line given in the Urick figure and the curve's non-linear behavior, as compared to the other more well behaved curves, indicates that the SUS signals at this depth are more complex than SUS dropped in deeper water.

In Figure 5, three plots **[Ref. 5]** illustrate SUS signal characteristics. This signal is for a charge of the same weight, but at a much deeper depth [102 m vs 18.2 m (60 feet)]. At the low frequencies of interest in this analysis, the long acoustic wavelengths are expected to complicate propagation and potentially bubble pulse development in the water depths examined **[Ref. 3]**.

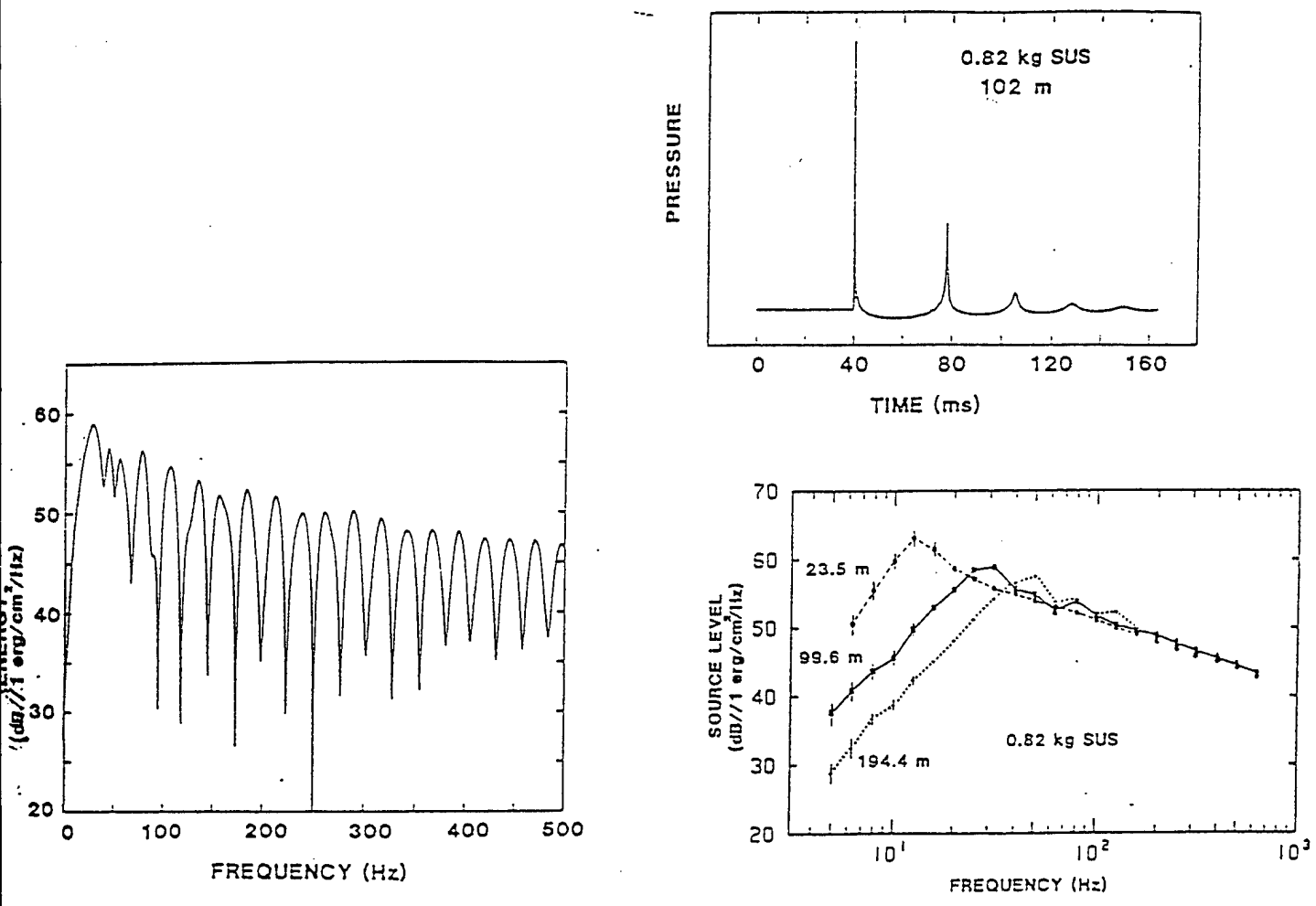

FIG. 2. Top: Waveform from the explosion of a 0.82-kg SUS charge at 102 m. The pressure series has been truncated after four bubble pulses to eliminate the surface reflection. Bottom: Energy density spectrum in dB *re*: 1 erg/cm²/Hz at 1 m for the waveform shown above.

FIG. 3. Source level measurements in 1/3 octave bands for 0.82-kg SUS charges at 23.5 m(●), 99.6 m(■), and 194.4 m(+). The error bars are standard deviations of the samples.

Figure 5. SUS Signal Characteristics.

The sonobuoys employed were all the attenuated AN/SSQ 57A model. Differing sonobuoy attenuations and the different source levels[4] at each octave were taken into account prior to reporting loss. The analysis of signal receptions was carried out in six octave bands which are given in Table 3 and shown graphically in Figure 6.

Octave	start-stop [Hz]	Bandwidth [Hz]	Center Freq.
1	17.2 - 35.9	18.7	26.6
2	35.9 - 70.3	34.4	53.1
3	70.3 - 140.6	70.3	105.5
4	140.6 - 282.8	142.2	211.7
5	282.8 - 565.5	282.8	424.2
6	565.6 - 1131.2	565.5	848.4

Table 3. Octave Bands.

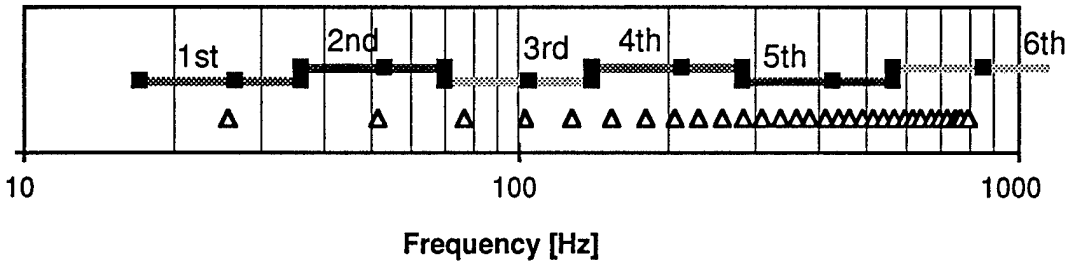

Figure 6. Log Plot of SUS Analysis Bands (with 'Sedi-layer' frequency maximums identified).

3. Results

3.1 Collected Data

The full SWAC-1 SUS data set is presented in Figure 7 and as Table A-1 in Appendix A. These data are the measured Total Energy transmission loss levels in each octave band. A spherical and cylindrical spreading curve, calculated using 68 + 10Log (range), is shown as a reference in Figure 7. The data at each octave

[4] SUS SL is not flat over the spectrum examined (as Figure 5 illustrates).

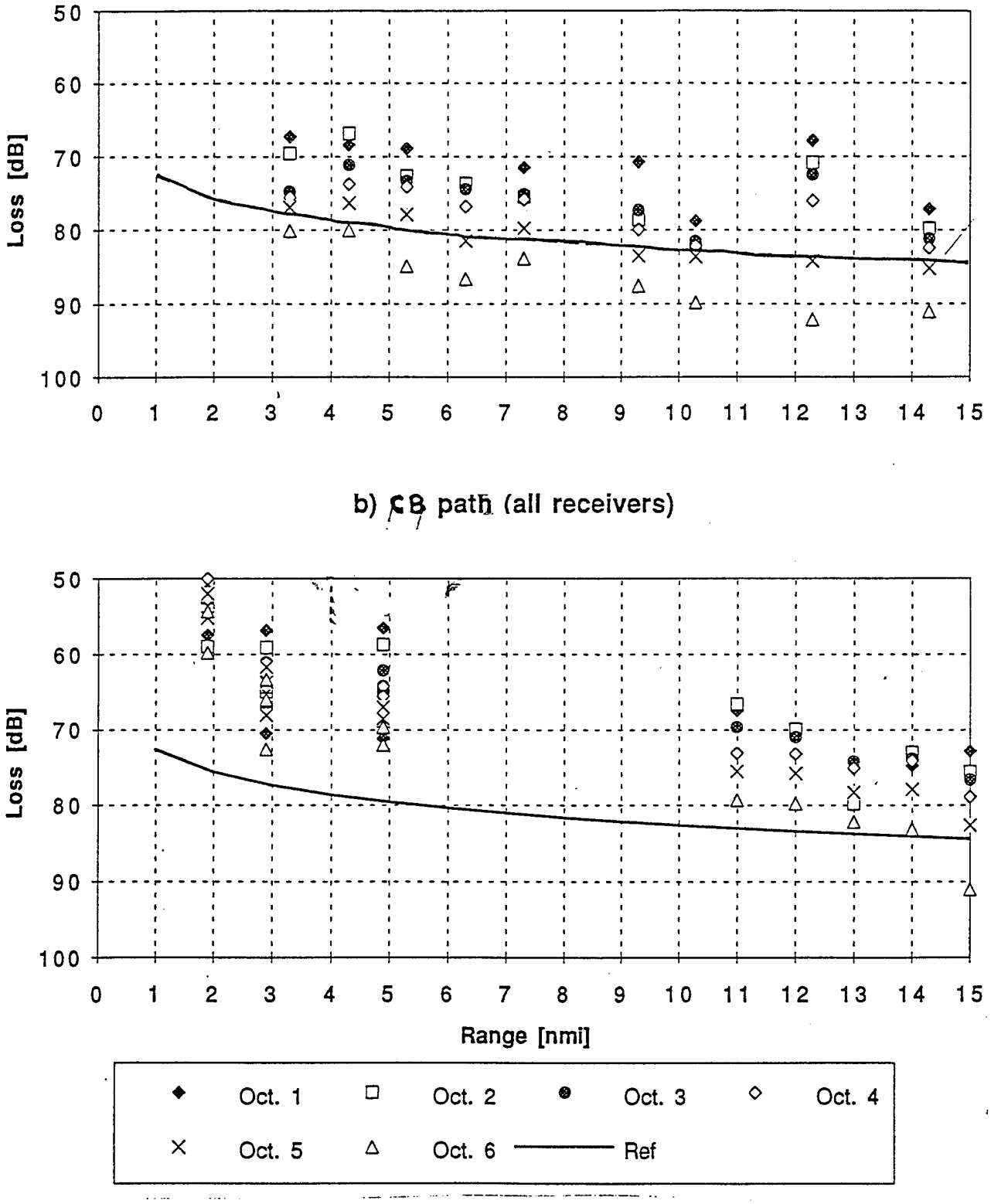

Figure 7 - SWAC data a) AB path and b) CB path.

follow the general trend of the reference curve and show a 10 to 22 dB difference in loss level from the first to final (high frequency) octave.

The data are organized for analysis into "Ping Averages vs Range" (average loss at all six octaves) and "Range Averages vs Octaves" (average loss across range interval) in Figure 8a and 8b. The range averages in Figure 8b are formed by considering the data received from sources between 0 and 5 nm (near range), 5 to 10 nm (mid range - AB only) and 10 to 15 nm (far range) to illuminate range-limited spectral effects, if any. (Note: The term "far range" is used relative to this data set and should not be confused with acoustic "far range" or "long range" propagation since 15 nm is still fairly close, acoustically.) The following observations are noted and will be explored in the analysis and modeling sections:

1) The AB path suffered 5 to 10 dB more loss than any of the CB paths in spite fact that the Test Plan predicts less bottom loss along the AB path. We note that the CB 'near range' distances are actually closer than the AB points (1.9, 2.9 & 4.9 nm vs 3.3, 4.3 & 5.3 nm), however Figure 7 clearly shows this is not the full explanation for the difference in loss level.

2) The deep receiver ("CB6 Near") on or in the bottom sediment layer, recorded less loss than the shallower (CB#4) receiver for the higher frequencies and more loss on the low frequencies as shown in Fig. 8b. "CB5 Near" also displays a similar effect, the flattening of the spectral distribution.

3) Shallow water propagation data typically displays an optimum frequency which is caused by increased attenuation with higher frequency and the wave guide's decreasing ability to trap low frequency energy. All of the SWAC data show higher attenuation with frequency, and with range. Only the #5 and #6 receivers (near range) register a significant loss of low frequency energy, favoring the 3rd and 4th octaves (centered on 100-200 Hz). The other data sets show some indication of increasing low frequency loss as propagation range increases.

a) Ping Average vs Range

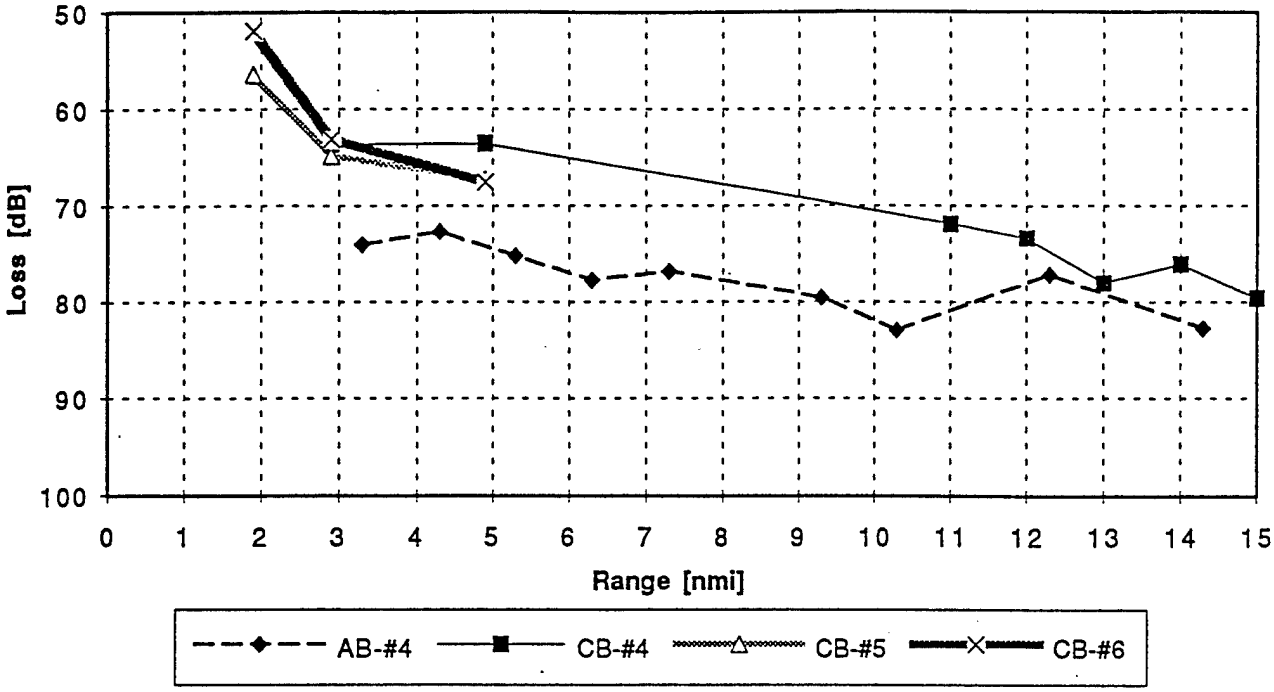

b) Average Values at each Octave

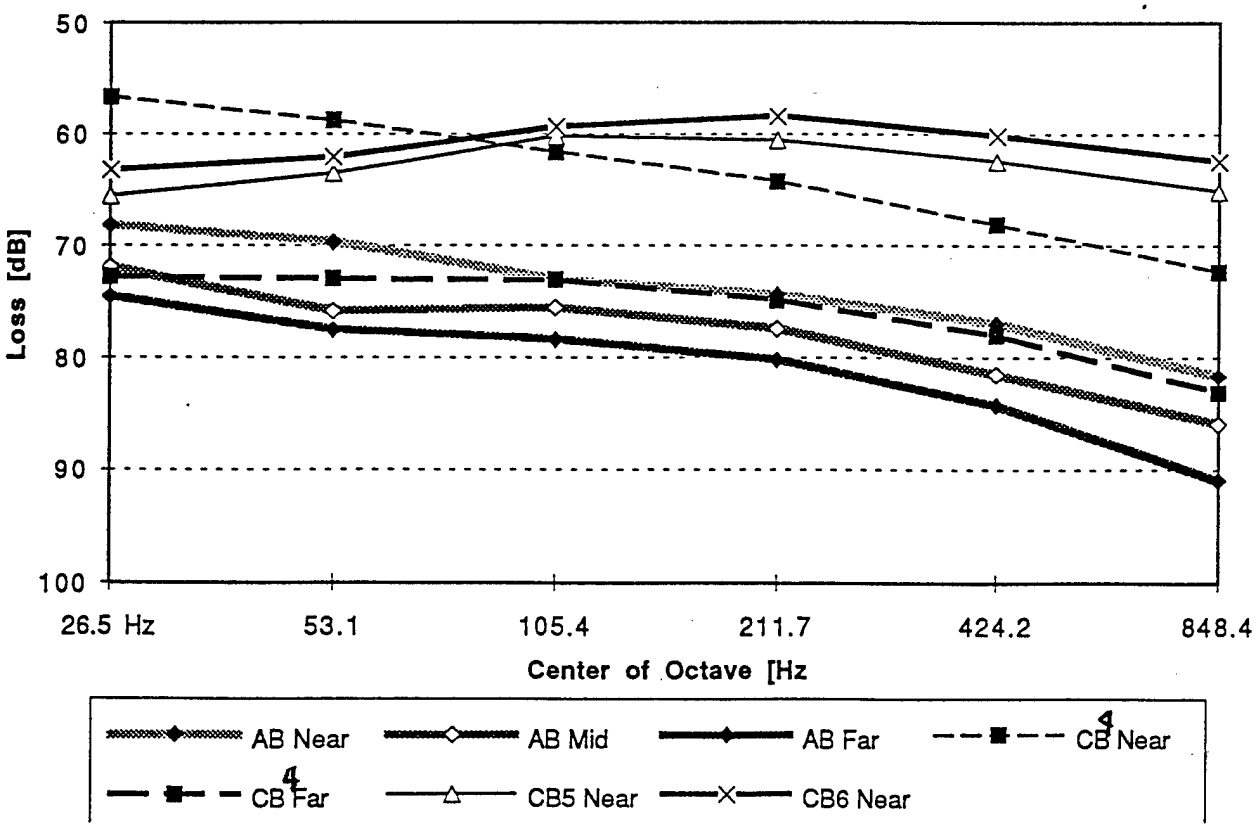

Figure 8. - SWAC data averages a) Average of all octaves and b) Average of range intervals.

3.2 Environment Analysis

The simple SSP and bottom bathymetries, described in the Introduction, are considered here. The SSP generally directs energy toward the bottom and intensifies the role of bottom interactions. The details of the bathymetry, for example the upslope and cross-slope components, modifys this transmitted energy and may account for the AB/CB path differences. The spectral character of the received signals are also examined in terms of general waveguide modes. Most of the data observations are supported by the environmental analysis. These observations are:

1) The upslope bathymetry of both tracks strongly affects the wide-angle acoustic propagation. Using ray trace analysis (which includes through-the-sediment propagation when the critical angle is exceeded) on the simplified SSP and bathymetry, the maximum angle for which rays can reach the receiver at B given their starting ranges are computed for each path. Figure 9a shows the percentage of an omni-directional beam which reaches the receiver for each of the paths. Figure 9b displays the associated angles and initial path types of the rays. (From a modal perspective, the upslope bathymetry forces the "angular" modes to slow down, dissipating energy to even higher angle modes which eventually leak out of the wave guide.) Assuming beam width relates directly to energy and all other conditions being nearly equal, nearly twice the energy is passed across the CB slope relative to the AB slope for the first half of the path. This supports the 5 to 10 dB additional loss observed in the AB data as compared to the BC data.

2) The downward refracting SSP directs and confines more energy to the lower water column layer in the profile. In general, receivers near the center of the a waveguide experience less loss. Both of these effects may explain the stronger propagation (high frequency) to the deep water receiver. We have no strong explanation for the additional loss of low frequency energy at these receivers.

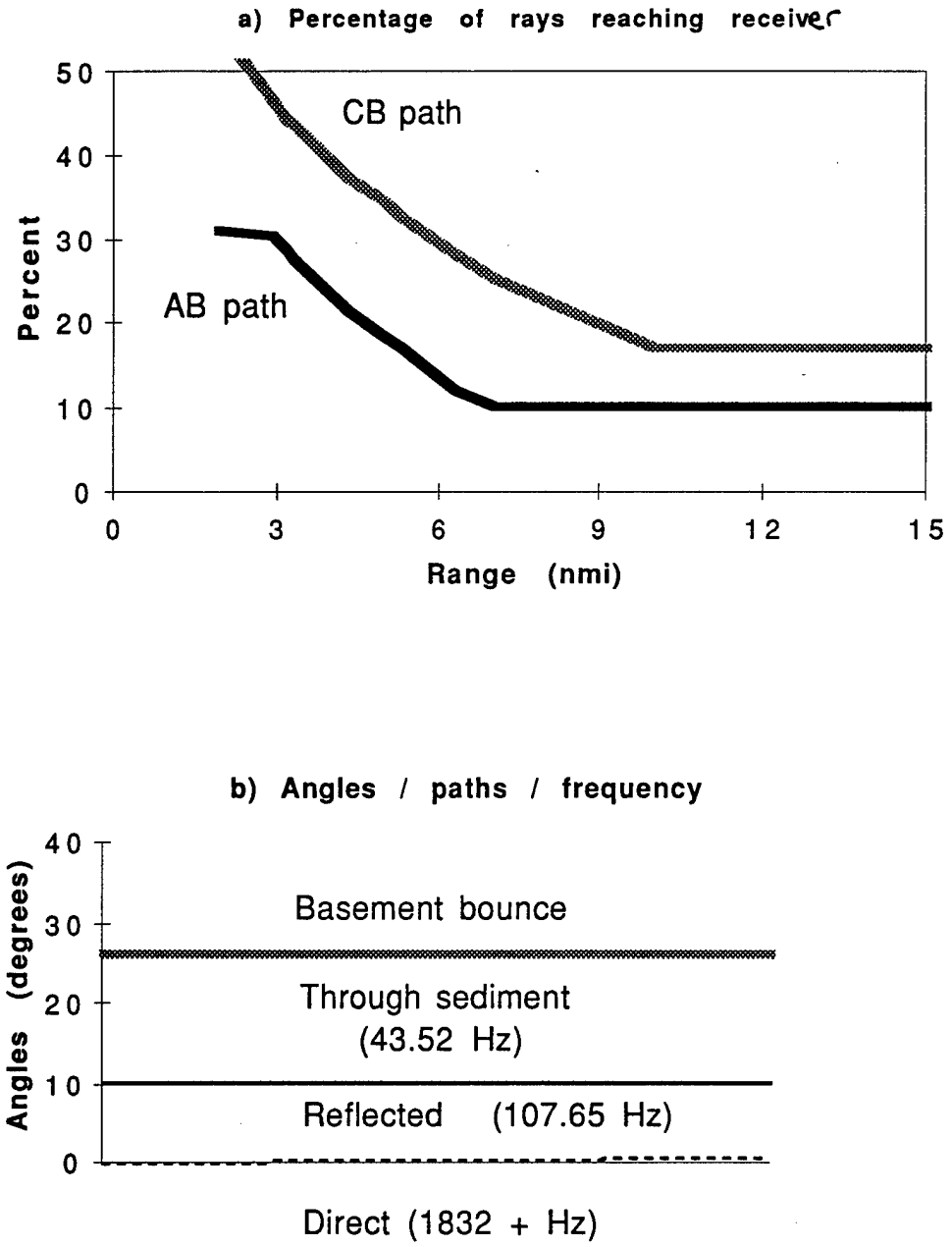

Figure 9. a) Percentage of rays (180° total) reaching receiver given simple bathymetry, SSP and through-the-sediment ray tracing, and b) corresponding angles, path types and estimated optimum frequency for each path.

3) The spectral character of the signal and the environmental effect on that character is an important issue in low frequency, shallow water acoustics. In the following analysis a continuous wave (CW) analysis is used to explore the spectral characteristics of the wave guide.

The shear wave sound speed of this sediment is 228 m/s or less, therefore there is no significant loss of energy due to shear wave conversion in this area. The cutoff frequency [f_{cutoff}=cw/(4*D*sqrt(1-(cb/cw)^2)) **Ref. 6**] for a wave guide overlaying a rigid basement is, at most, 7.675 Hz for the 135m depths in the area. Although actual sediment and basement parameters may increase these frequencies somewhat, they are well below the first octave in this experiment and therefore frequency cutoff is not a player in the observed propagation.

Optimum frequencies normally occur between 200 and 800 Hz in shallow water depths of 100m **[Ref. 6].** They are estimated for this environment by considering the 'least lossy' Lloyd's mirror beam over a range independent (RI) environment. (The 'least lossy' beam also relates to the strongest trapped normal mode of the wave guide). The optimum frequency estimate equation used, f_{opt} = co/(4*zs*sin(critical/grazing angle) **[Ref. 6]**, provides the values in Figure 9b for various 'channeled wave guides'. The direct and purely water-borne (from 0 degrees to 0.02 min/0.65 max degrees) energy is insignificant. The sediment reflected path and the through-the-sediment angles both point to a lower optimum frequency than the typical 200-800 Hz values. The 100 Hz band is favored in the analysis (and is supported by the data observations) although the upslope bathymetry may force some of this low frequency energy into the sediment paths.

Range dependence (RD) in the environment, tends to obscure the formation of optimum frequencies **[Ref. 7]** and the prediction of optimum frequencies is difficult. The near range sources may see a shallow wave guide (40-100 Hz) which is close to range independent (RI) over short ranges. But short ranges are not sufficient to filter out the leaky modes. The far range propagation initially experiences a range independent deep water channel which will tend to select the 100 Hz frequency. Upon encounter of the slope, however, energy from this mode will be forced into the sediment modes and may revive the 40 Hz energies, effectively sustaining them for short distances. If the bottom depth behind B, were level and contained receivers, one would expect the 40 Hz energies to fall off and the dominant energy return to the 100 Hz value.

Finally, the basement bounce rays which experience a high number of surface and bottom interactions, accumulate a large amount of loss at each bounce, as well as the "geometric attenuation" cancellation presented in section 1. The high loss is somewhat mitigated at particular frequencies and angles where the sediment reflection and bottom reflection constructively interfere. Assuming a constant average sediment sound speed of 1670 m/s, these frequencies were calculated and are indicated by triangles on Figure 6. The values fall in the middle of the low octave bandwidths, perhaps strengthening the response at these lower center frequencies and counteracting low frequency leakage.

3.3 Modeling Analysis

Three RD acoustic propagation prediction programs, Parabolic Equation (PE), ASTRAL and Comprehensive Acoustic Sonar Simulation (CASS) **[Refs. 8-10]**, are used to model the propagation in the SWAC region. Each of these models was developed primarily for deep water, CW propagation. Each model approaches the problem from a different theoretical viewpoint. PE is a parabolic equation program, ASTRAL is based on modal theory and GRAB (Gaussian Ray Acoustic Bundles, a transmisison loss model within CASS) uses gaussian ray tracing. First a basic description of the models and environmental sensitivity tests are presented, then predictions for each of the experimental paths are compared with the received datasets.

PE and ASTRAL were exercised under the CAAM 4.0 **[Ref. 2]** interface which allows the use of historical or user-defined SSPs. All other environmental information is obtained from historical databases or defaulted. Both use the unstarred parameters of the bottom model described in Table 2 **[Ref. 11]**.

The CASS model was exercised under the CAAM 4.0 interface and as a stand alone model where inputs can be fully manipulated. The RD eigenray model, GRAB , was employed for all predictions. Bottom reflection tables based on the unstarred geoacoustic parameters (Table 2) were generated for the CASS runs. No corrections for 'through-the-sediment' paths were made. Results using CASS on a "fluid sediment layer" are presented in Appendix B.

PE is often the model of choice for low frequency, range dependent environments. The sensitivity tests and model/data analysis use the PE results to illustrate predictions when all models are in general agreement.

ASTRAL has a shallow water limit of D = 13 to 20 lambda (which is almost centered on the SWAC conditions) beyond which results are considered unreliable. In addition, ASTRAL assumes a slowly varying environment where mode coupling is insignificant. For these reasons, the ASTRAL predictions must be carefully scrutinized.

CASS has not been, to our knowledge, exercised or tested on low-frequency, shallow water environments. Although the ray tracing approach has difficulties in accounting for sediment effects and modal characteristics, it is adept at handling complex range dependent problems especially where the environment is rapidly changing.

The models were run on the octave center frequency (CASS on lowest, mid-2 and highest octaves) without any bandwidth or pulse post processing. All model runs presented use the *in situ* SSP generated for pod B unless otherwise noted. Differences between the pod A and pod B profile predictions were negligible for all models and tracks.

The principle of reciprocity was brought to bear to simplify the modeling process. Reciprocity was tested at both 'near' and 'far' ranges for each of the models in each of the acoustic tracks (also near bottom receiver). Differences ranged from less than 2 dB (CASS) up to 5 dB (PE & ASTRAL low-mid frequencies) on most of these tests. The longer ranges and higher frequencies tended to display the greatest differences in the reciprocity tests for all models. The differences in the high ASTRAL frequencies (424.2 & 848.4 Hz) exceeded 15-25 dB. The upslope ASTRAL spectral predictions were basically flat.

The historical sound speed profile predictions available under CAAM differed from the *in situ* profile results primarily in the upper layer as shown in Figure 10a. Predictions using the historical profile along the BC path differed as much as 10 dB in magnitude for particular frequencies and ranges as well as modified the 'structural' definition of the results, Figure 10b. Low frequencies experienced the least change (less that 2 dB PE, 3 dB ASTRAL shallow and 5 dB ASTRAL deep).

Bathymetry effects are gauged using a nearly flat bottom bathymetry at approximately 150 and 350 ft. These RI predictions are shown against the range dependent (RD) prediction in Figure 11. In general, the RD predictions follow the 150 ft RI loss curve out to about 5 nm before flattening out and migrating

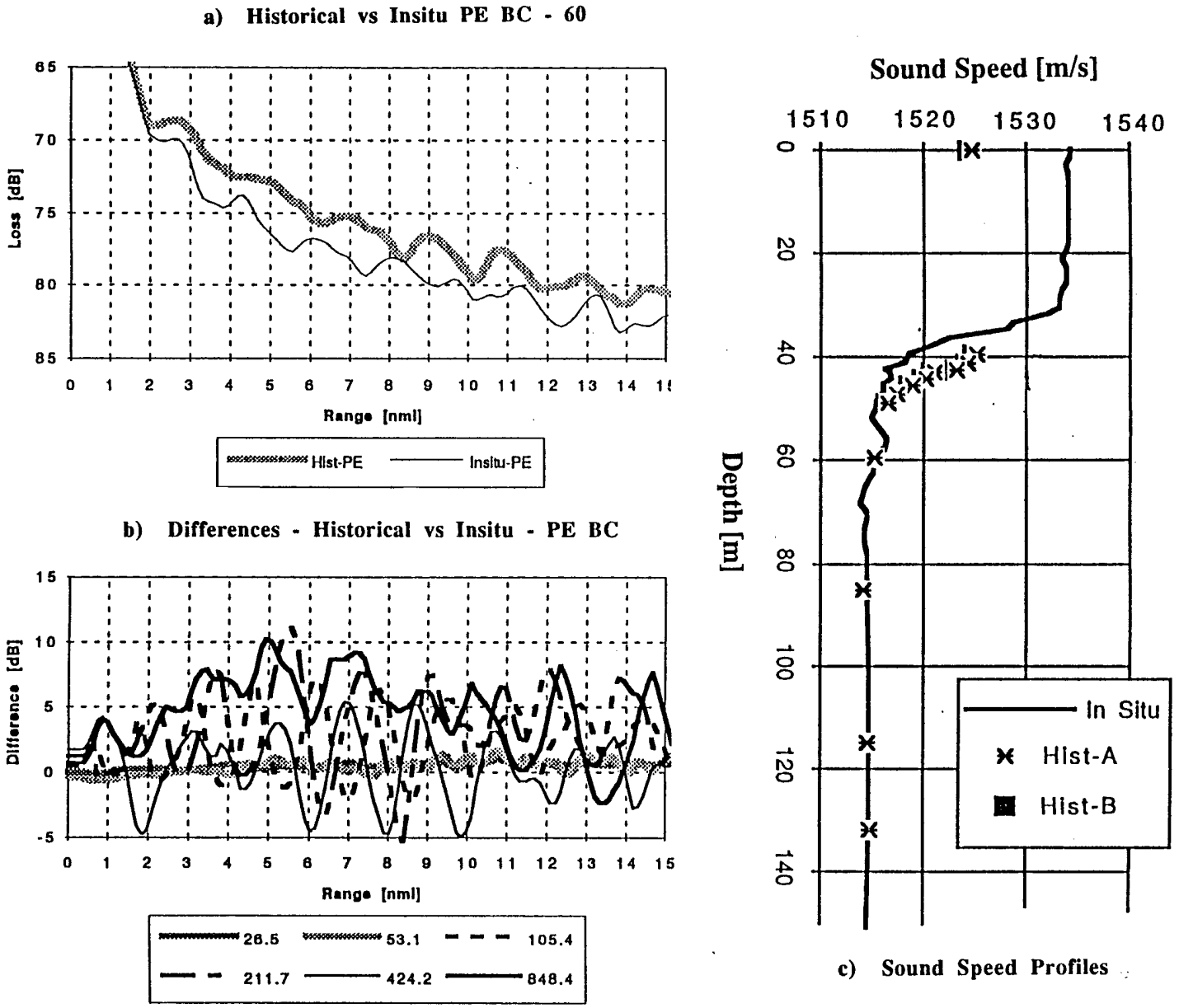

Figure 10. Historical vs Insitu Profiles (at site B) - a) PE Ping Averages for BC path, shallow receiver; b) Differences (Hist - Insitu) for each frequency against range; and c) Sound Speed Profiles.

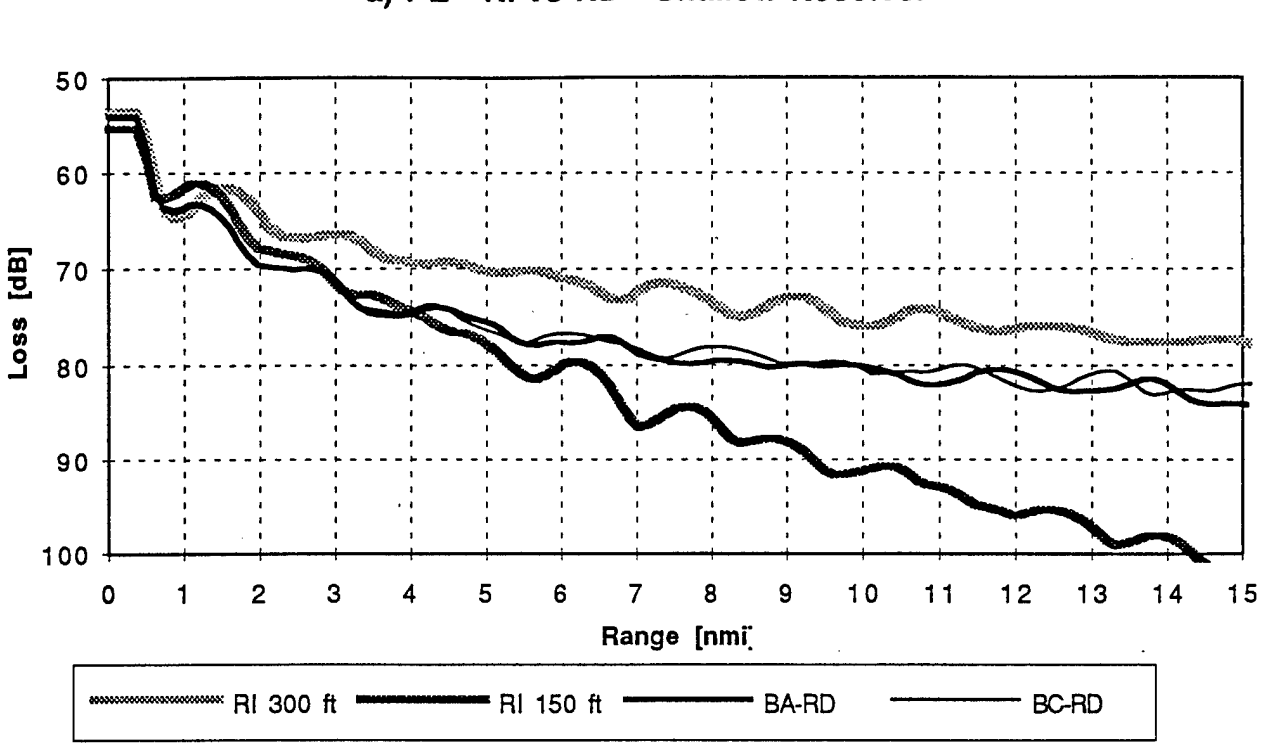

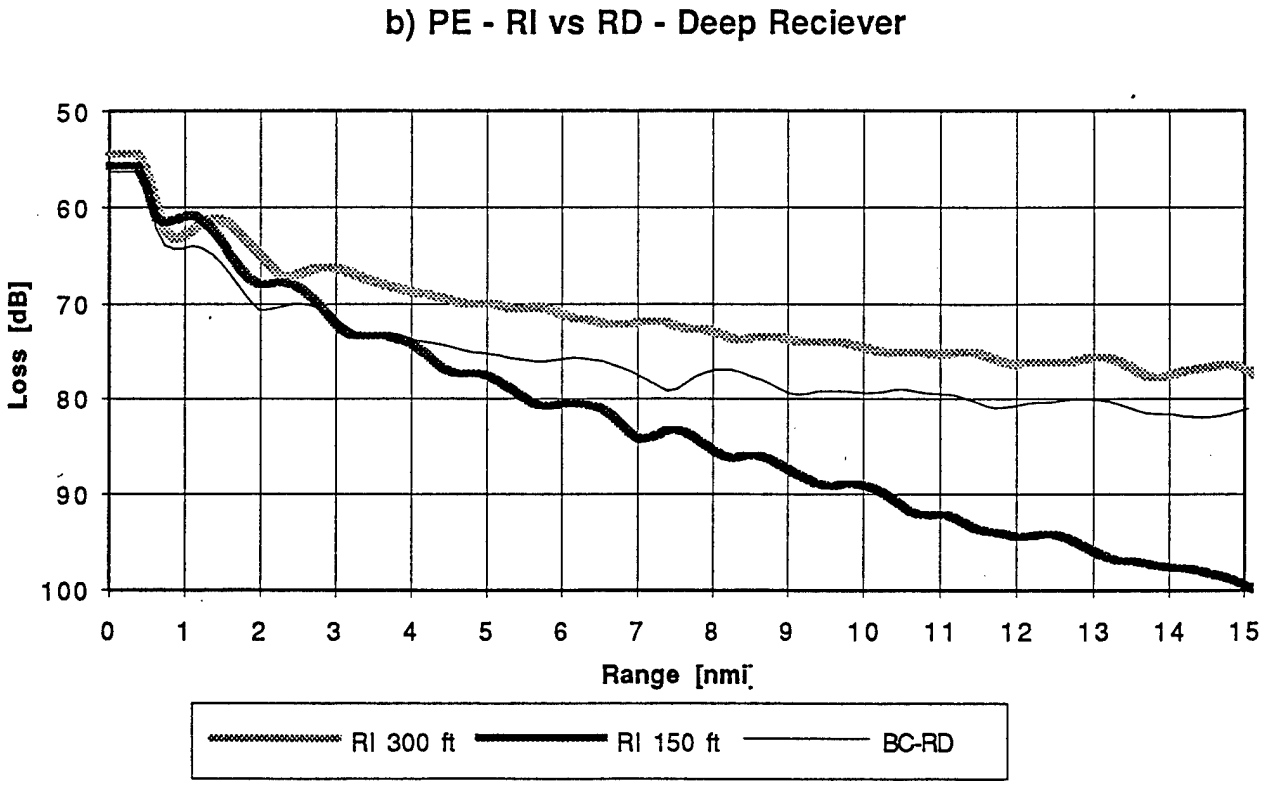

Figure 11. Flat bottom (150 & 300 ft) vs Range Dependent PE predictions on BC path using a) shallow (60 ft) and b) deep (150 ft) receivers.

closer to the 300 ft RI propagation loss curve at the far ranges. This behavior is consistent with the environmental analysis and expectations.

No significant spectral differences were observed in these tests. Although the formation of the 100 Hz optimal frequency is clearly demonstrated in the range independent predictions.

3.4 Data/Predictions Comparisons

All three models were exercised on the two SWAC paths (AB & CB) with a shallow receiver and on the BC deep receiver path. The results are summarized in Figures 12, 13 and 14. The full set of predictions can be found in Appendix C. The results were compared with the SWAC data and particular examples were selected to illustrate or analyze the particular observations made.

1) The SWAC data set indicates that the AB path experiences more loss than the CB path at comparable ranges. Only ASTRAL predicted significantly more loss (about 5 dB) for the AB path (Figure 12 and 13).

2) The deep receiver on the CB path consistently records a stronger signal (approx. 10 dB) than the shallow receiver during the test. All models agreed (approx 5 dB - PE, up to 20 dB - ASTRAL, 10 dB - CASS). None of the models exhibited the spectral differences observed in data. PE predicts a flatter spectrum, as observed in the data (Figures 13 and 14).

3) As previously mentioned, the SWAC data and simple wave guide analysis points to optimum frequencies lower than the general 200-800 Hz. The ASTRAL acoustic propagation model favors the very low frequency (26.5 and 53.1 Hz). PE indicates lowest losses at 100 and 400 Hz. CASS, which does not model through the sediment propagation, displays very little change for frequencies less than 848.4 Hz (the "thro-the-sedi" runs in Appendix B, show some low frequency attenuation).

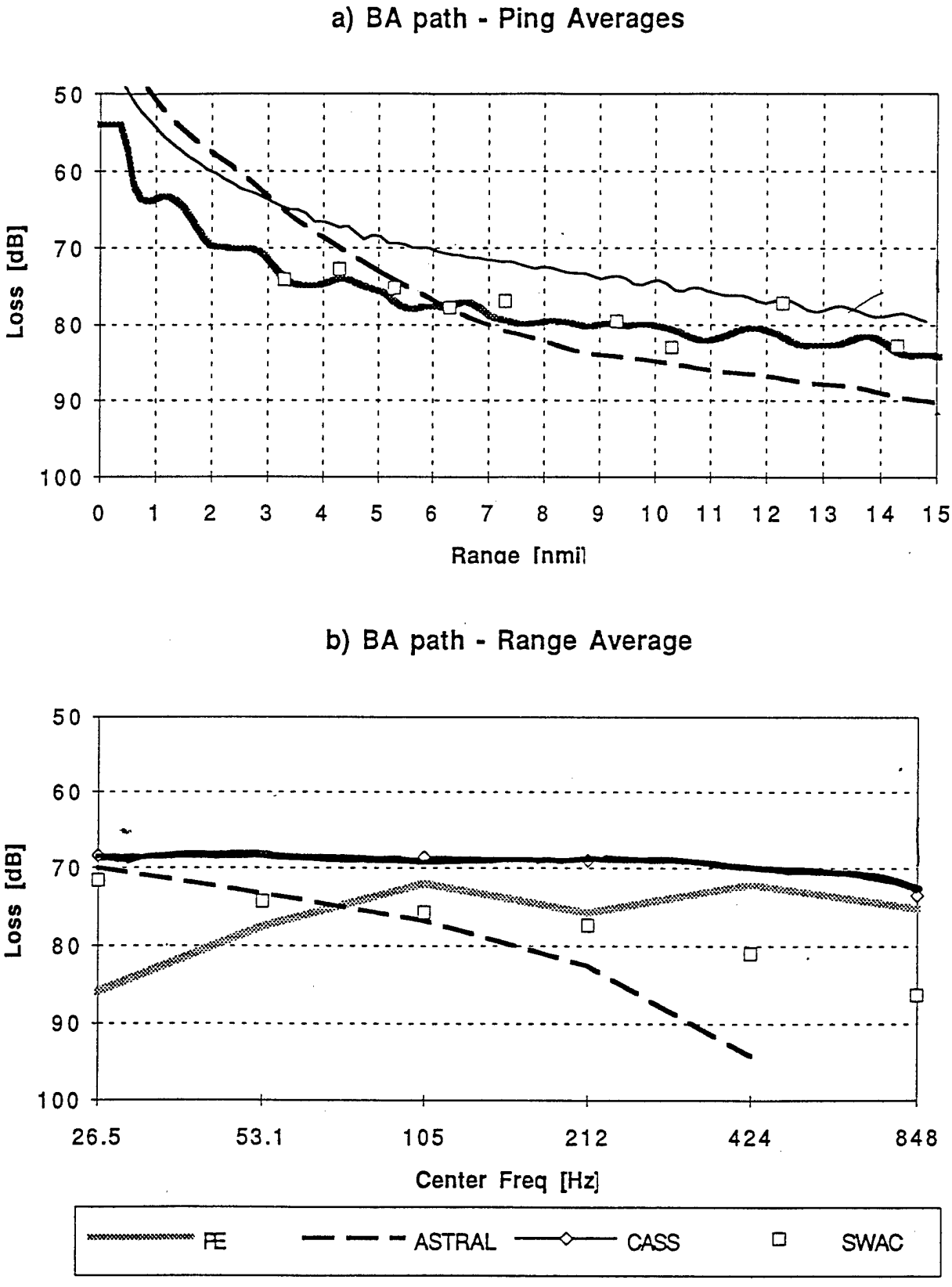

Figure 12. Model (PE, ASTRAL & CASS) Predictions vs SWAC data on the BA path - a) Ping Averages and b) Range Averages (shallow receiver).

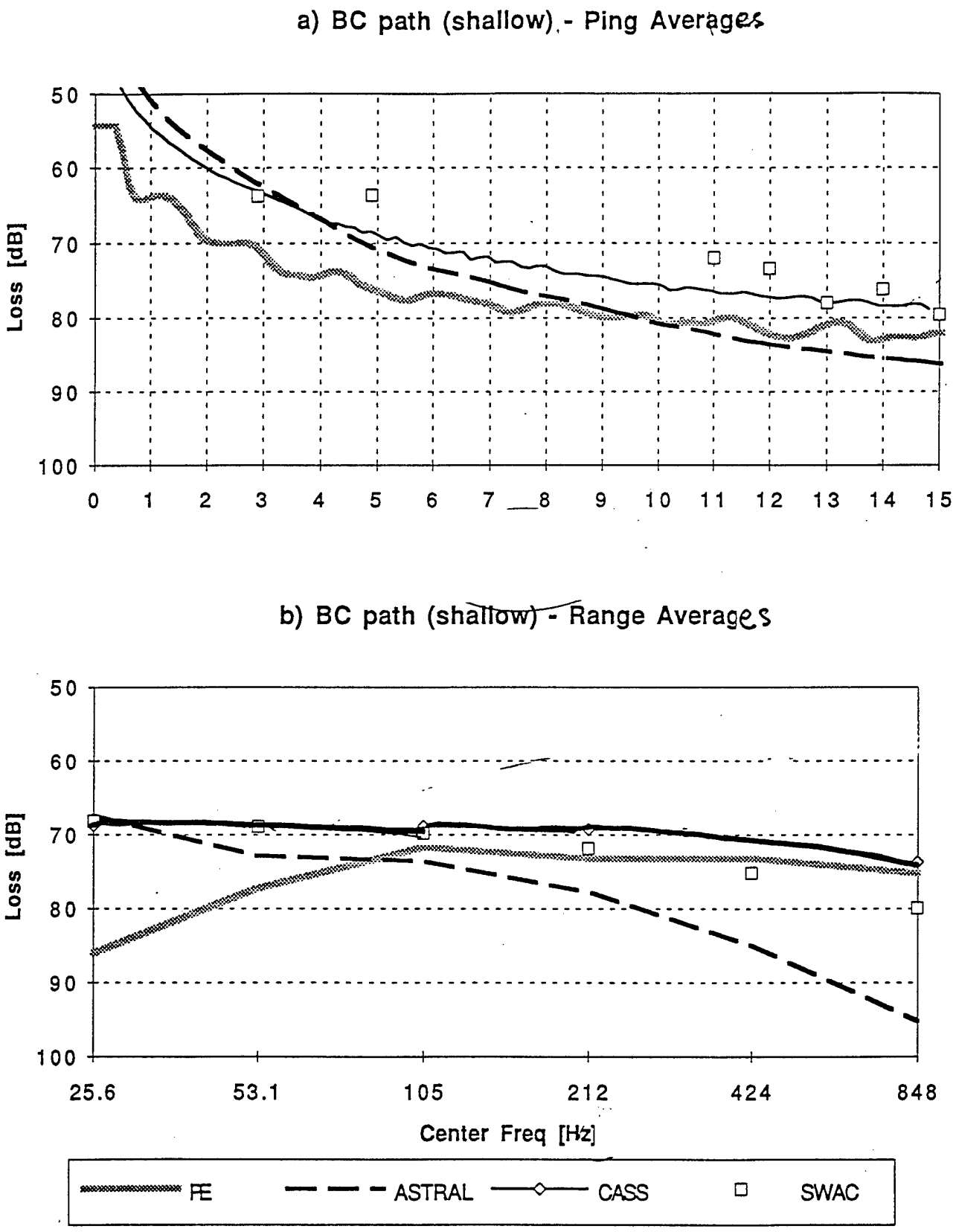

Figure 13. Model (PE, ASTRAL & CASS) Predictions vs SWAC data on the BC path - a) Ping Averages and b) Range Averages (shallow receiver).

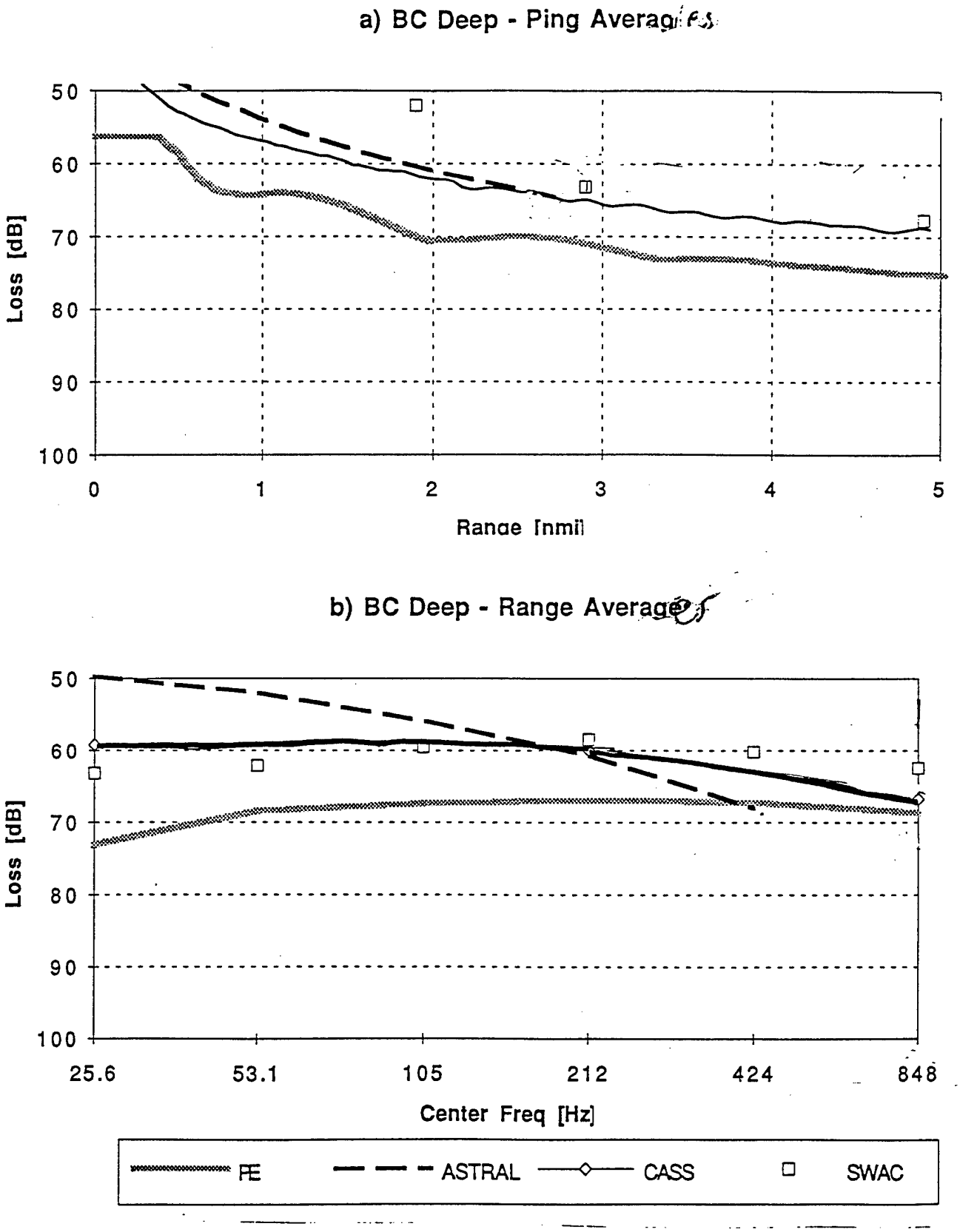

Figure 14. Model (PE, ASTRAL & CASS) Predictions vs SWAC data on the BC path using a deep (150 ft) receiver - a) Ping Averages and b) Range Averages.

4. Conclusions

4.1 The impulsive SUS signal differs in many ways from CW signals (commonly used in models) and HFM or LFM signals used elsewhere for environmental work at these frequencies. Not only do the signals differ, but the processing algorithms also differ. Relating results from SUS to that of other signal types, such as an extrapolation to HFM results, will require further research.

4.2 Low frequency shallow water propagation prediction is not yet as well developed as the capabilities in deep water. Littoral waters present difficulties for models in the availability of ample and accurate environmental inputs and in the modeling of the known effects (such as mode conversion and ray splitting). Additionally, the following contributes to the modeling difficulty:

a). High resolution bathymetry in this shallow water area was not readily available (note the blanked area in Figure 2). To enable prediction in such areas this information is absolutely needed.

b). Although geo acoustic parameters for the sediment layer were available for this general region, information like this is not easily obtained. Shear sound speeds for the area (although they can not be utilized by all models) were not available from the database. They were developed from the general descriptions used and other acoustic surveys. This may be a significant source of loss in shallow water propagation, with the added complication of frequency dependence.

c). Few, if any, propagation models have been fully tested (proven) for low frequency in littoral environments. The adaptation of deep water models to the task has yet to be proven effective.

4.3 Although some trends in the measured data are observed, this particular data set is small. There are uncertainties regarding the exact source signal, depth of detonation and location as well as some uncertainties in the location and depths of the receivers. A greater sample of the area would be needed to draw conclusions which are less tentative. A recommendation is that collection of comprehensive, well detailed propagation data sets for model comparison and validation continue.

4.4 Given the concerns voiced above, the acoustic analysis of the area's environmental parameters generally supports the observations in the data set. This support could be strengthened with better knowledge of the inputs (bottom and sub bottom characteristics as well as better sampling of the local sound speed field). Additionally, littoral models which can utilize all of the available environmental inputs, and have been proven in shallow water are not yet as good as deep water models.

Acknowledgments

We would like to thank the SWAC program and its participants for copies of reports and the use of these data. Additionally, we wish to acknowledge Naval Undersea Warfare Center for the use of the USWAL facilities in running the prediction systems of CAAM and CASS.

References

1. Shallow Water Active Classification-1 (SWAC-1) Sea Trial; 18 Oct-9 Nov 1994 Quicklook Report", NUWC, SACLANTCEN, NAWC, NCCOSC, NRL, NUWC-NPT Tech Memo 951004, 16 January 1995.

2. Composite Area Analysis Model (CAAM) 4.0
"CAAM User's Guide",28 July, 1995, Sonalysts, Inc., 215 Parkway North, Waterford, CT 06385.
GEM databases from OAML:
   - XBT databases v1.0 July '86 from SIMAS v2.0
   - DBDB2 - March '92, LFBL 4.0 May '92

3. "SUS Charge Sources", p 119-122 in the ARSRP Initial Report, 19 August 1991.

4. "Principles of Underwater Sound", Second Edition, Robert J. Urick, 1975.

5. "Source levels of shallow explosive charges," N. R. Chapman, J. Acoust. Soc. Am, 84 (2) (p697-702), August 1988. see also: "Measurements of the waveform parameters of shallow explosive charges," N. Ross Chapman, J. Acoust. Soc. Am, 78 (2) (p672-681), August 1985.

6. Jensen, Kuperman, Porter, Schmidt, Computational Ocean Acoustics, AIP Press, NY 1994.

7. Jean-Pierre Hermand, Raymond J. Soukup, "Broadband inversion experiment Yellow Shark '95: Modeling the transfer function of a shallow-water environment with range-dependent soft clay bottom", 3rd European Conference on Underwater Acoustic, 24-28 June 1996, Heraklion Crete, Greece and to be published in Proceedings of the 3rd European Conference on Underwater Acoustics.

8. Holmes, E.S. and L.A. Gainey, "Software Requirements Specification for the Parabolic Equation Model Version 3.4," OAML-SRS-22, Ocean and Atmospheric Master Library, Naval Oceanographic Office, Stennis Space Center, MS, July 1992. [version 3.3 actually used in predictions]

9. ASTRAL 2.4e was used.
Spofford, C.W., "The ASTRAL Model Volume I: Technical Description," Sci. Appl., Inc., SAI-79-742-WA (Jan 1979), and:
- D. White and R.J. Moore," Software Design Description for the ASTRAL Model," OAML-SDD-23, Ocean and Atmospheric Master Library, Naval Oceanographic Office, Stennis Space Center, MS, 1991.
- White, D. and Corely, M., "Software Design Document for the ASTRAL Model (Version 4.1)," Sci. Appl. Inter. Corp., OAML-SDD-23 (Oct. 1992)

10. CASS Reference Guide, Henry Weinberg, NUWC Div., NL, 06320, 17 February 1994. see also Ref 2: CAAM 4.0 User's Guide

11. "Input Parameters for Acoustic Model Comparisons . . .", Emily McCarthy, MAI 207-3-94 EHM-04.

Appendices

A. SWAC Data

B. Historical, RI Model Sensitivity Results

C. Model Runs used in the Main Text

APPENDIX A: SWAC DATA

The data collected and processed by NAWC is presented in the two tables which follow. The sonobuoy is identified by the A to D channel.

C to B track (SUS dropped every nmi)
* buoys listed here were at site B.

A to D Chan	Range (nmi)	Octave: 1	2	3	4	5	6	Average loss across all octaves C-B
4(60')	15	72.91	75.67	76.75	78.94	82.66	91.05	79.66
4(60')	14	74.78	73.06	73.88	74.12	77.98	83.16	76.16
4(60')	13	78.5	79.85	74.34	75.16	78.38	82.15	78.06
4(60')	12	70.62	69.99	71.04	73.31	75.82	79.74	73.42
4(60')	11	67.46	66.57	69.72	73.16	75.53	79.38	71.97
4(60')	4.9	56.57	58.71	62.2	64.23	68.23	72.08	63.67
5(60')	4.9	68.92	67.59	64.19	65.52	68.55	69.65	67.40
6(btm)	4.9	71.14	68.86	65.05	64.25	66.96	69.77	67.67
4(60')	2.9	56.88	59.09	61.11	64.37	68.1	72.71	63.71
5(60')	2.9	70.51	64.26	61.65	63.52	63.67	66	64.94
6(btm)	2.9	67.06	64.94	61.47	61.13	61.64	63.27	63.25
6(btm)	1.9	51.6	52.56	51.81	49.98	51.97	54.3	52.04
5(60')	1.9	57.44	58.9	55.04	52.79	55.23	59.78	56.53
Ave. loss in octave:		66.49	66.16	65.25	66.19	68.82	72.54	

Note: a 400' sonobuoy was deployed (6) but the local bathy. was about 160'.

Difference between 60' and btm receivers at each octave
(- indicates that the bottomed sonobuoy experienced greater loss)

nmi						
1.9	5.84	6.34	3.23	2.81	3.26	5.48
2.9	-3.365	-3.265	-0.09	2.815	4.245	6.085
4.9	-8.395	-5.71	-1.855	0.625	1.43	1.095

Table of C to B data and statistics.

A to D Chan	Range (nmi)	A to B track (SUS dropped every nmi) Octave: 1	2	3	4	5	6	Average loss across all octaves A-B
4(60')	3.3	67.3	69.56	74.89	75.59	76.93	80.09	74.06
4(60')	4.3	68.43	66.9	71.2	73.73	76.35	80.03	72.77
4(60')	5.3	68.88	72.63	73.36	74.16	77.87	84.86	75.29
4(60')	6.3	73.75	73.69	74.46	76.83	81.49	86.55	77.80
4(60')	7.3	71.53	75.48	75.15	75.82	79.75	83.89	76.94
4(60')	9.3	70.74	78.57	77.37	79.9	83.49	87.54	79.60
4(60')	10.3	78.82	82.02	81.61	82.22	83.64	89.87	83.03
4(60')	12.3	67.77	70.88	72.47	76.06	84.11	92.08	77.23
4(60')	14.3	77.14	79.85	81.22	82.47	85.24	91.13	82.84
Ave. loss in octave:		71.60	74.40	75.75	77.42	80.99	86.23	

Table of A to B data and statistics.

Appendix B: Historical, RI Model Sensitivity Results

Prior to modeling the SWAC scenario, various tests were performed to gauge model sensitivity in the area to unknown or uncertain parameters. The key results are presented in this appendix.

PE full field plots are included to illustrate receiver depth sensitivity. To explore the "through the sediment" contributions an alternative fluid sediment layer was developed for the CASS model. This used a sound speed profile which extends into the sediment layer as represented in Figure 3(c); a depth/frequency dependent attenuation table and a bottom (basement) reflection coefficient of -1.0 (perfectly reflecting).

The attenuation coefficients for each center frequency was computed using Thorpe for the water column and the conservative assumption that the attenuation coefficient is proportional to frequency. A reference value of 63 dB/km @ 100 Hz was used in the latter computation. A simple bathymetric model was employed for each path and attenuation tables inserted at each turning point.

Particular loss differed from the "sediment reflection representation" by less than 2 dB, supporting the conclusion that this thin sediment layer need not be fully accounted for in this environment. These averaged shallow water results are virtually identical to the results using a sediment/bottom reflection coefficient value differing by less than 2 dB. The "through the sediment" loss curves showed more variation (structure) in the higher frequencies. There was also more low frequency loss in the far range.

Figures B-1 through B-4

Since a large number of model runs were made, these PE curves show averaged results. One set of averages shows all pings (ping averages) and the other shows frequency dependence for three sub-segments of the range over which measurements were made (0-5 nm, 5-10 nm, 10-15 nm).

Figure B-1: PE range independent results using a flat bottom assumption, a shallow SUS and a 60 foot receiver.

Figure B-2: PE range independent results using a flat bottom assumption, a deep SUS and a 60 foot receiver.

Figure B-3: PE range independent results using a flat bottom assumption, a shallow SUS and a 150 foot receiver.

Figure B-4: PE range independent results using a flat bottom assumption, a deep SUS and a 150 foot receiver.

Figure B-5: PE results for the C to B path showing depth sensitivity at 26.5 Hz (top plot) and 848.4 Hz (bottom plot).

Figure B-6: Same prediction as Figure B-5 showing results at closer range.

Figures B-7 through B-9

As in Figures B-1 through 4, averages are used to explore parameteric effects. This time, however, the CASS model is employed.

Figure B-7: Cass prediction along the BA path with a shallow receiver.

Figure B-8: Cass prediction along the BC path with a shallow receiver.

Figure B-9: Cass prediction along the BC path with a deep receiver.

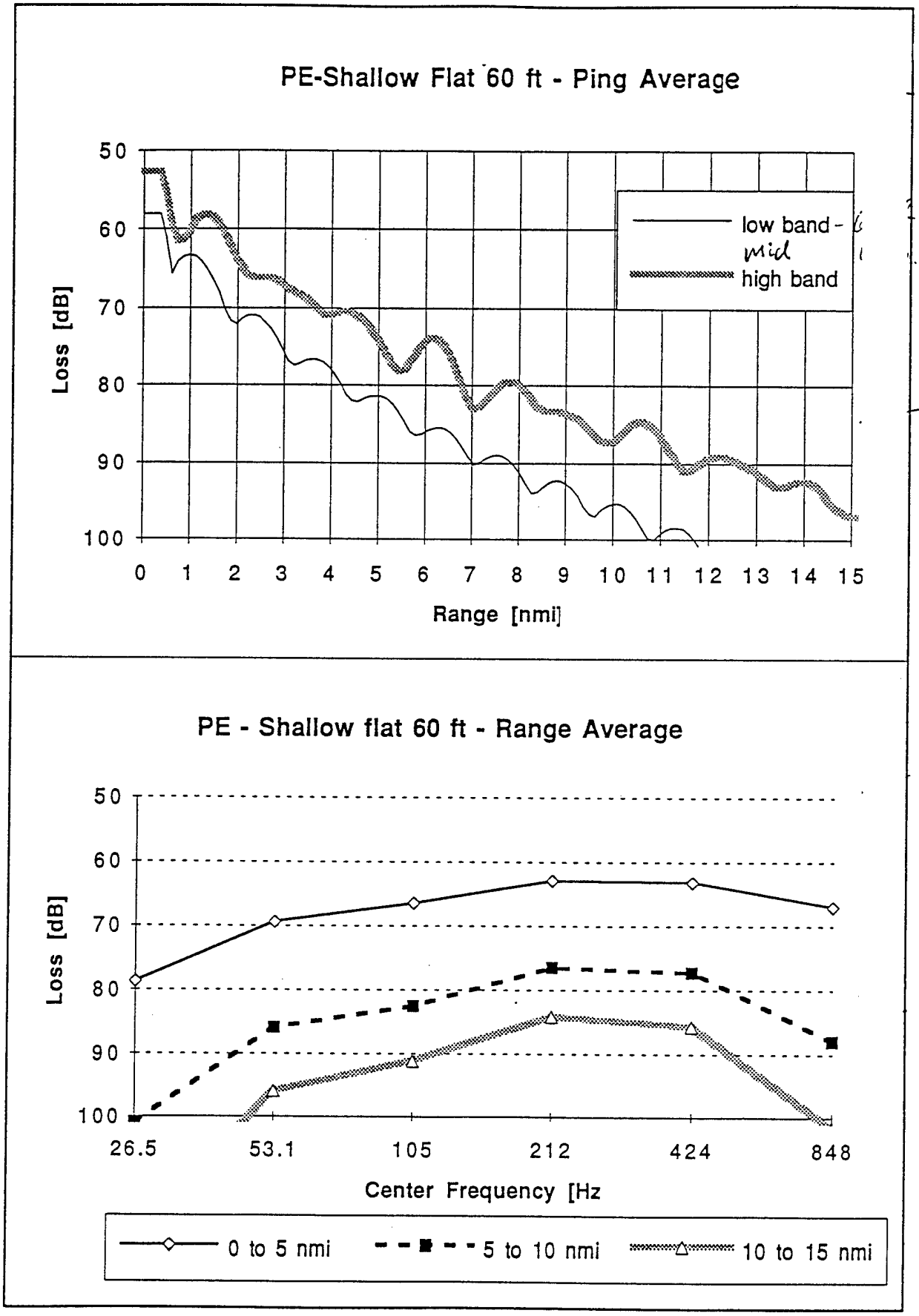
PE-Shallow Flat 60 ft - Ping Average
Loss [dB]
50
60
70
80
90
100
0 1 2 3 4 5 6 7 8 9 10 11 12 13 14 15
Range [nmi]
low band -
mid
high band
PE - Shallow flat 60 ft - Range Average
Loss [dB]
50
60
70
80
90
100
26.5
53.1
105
212
424
848
Center Frequency [Hz
0 to 5 nmi
5 to 10 nmi
10 to 15 nmi

Figure B-1

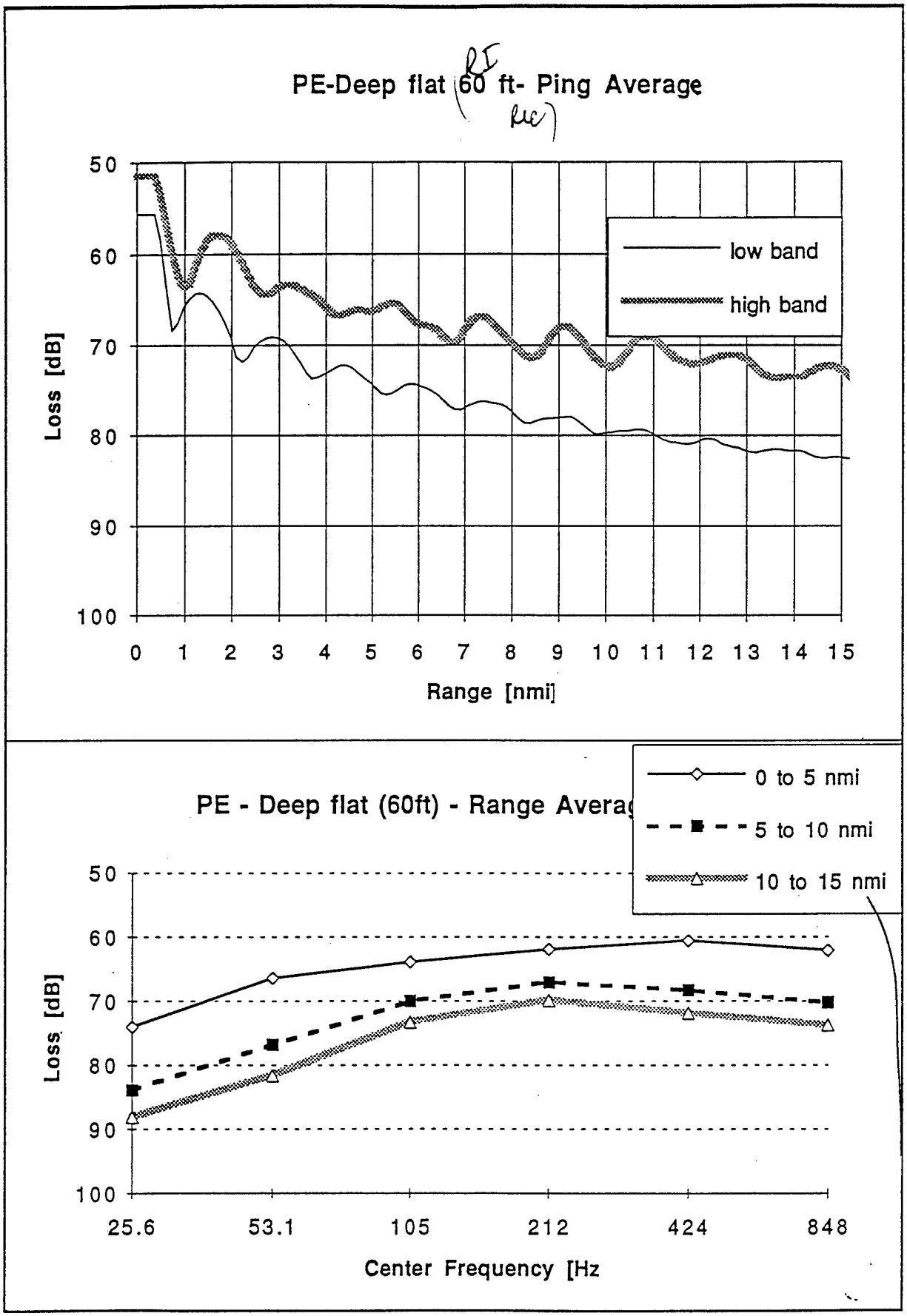
PE-Deep flat (60 ft- Ping Average
50
60
70
80
90
100
Loss [dB]
0 1 2 3 4 5 6 7 8 9 10 11 12 13 14 15
Range [nmi]
low band
high band
PE - Deep flat (60ft) - Range Averag
0 to 5 nmi
5 to 10 nmi
10 to 15 nmi
50
60
70
80
90
100
Loss [dB]
25.6
53.1
105
212
424
848
Center Frequency [Hz

Figure B-2

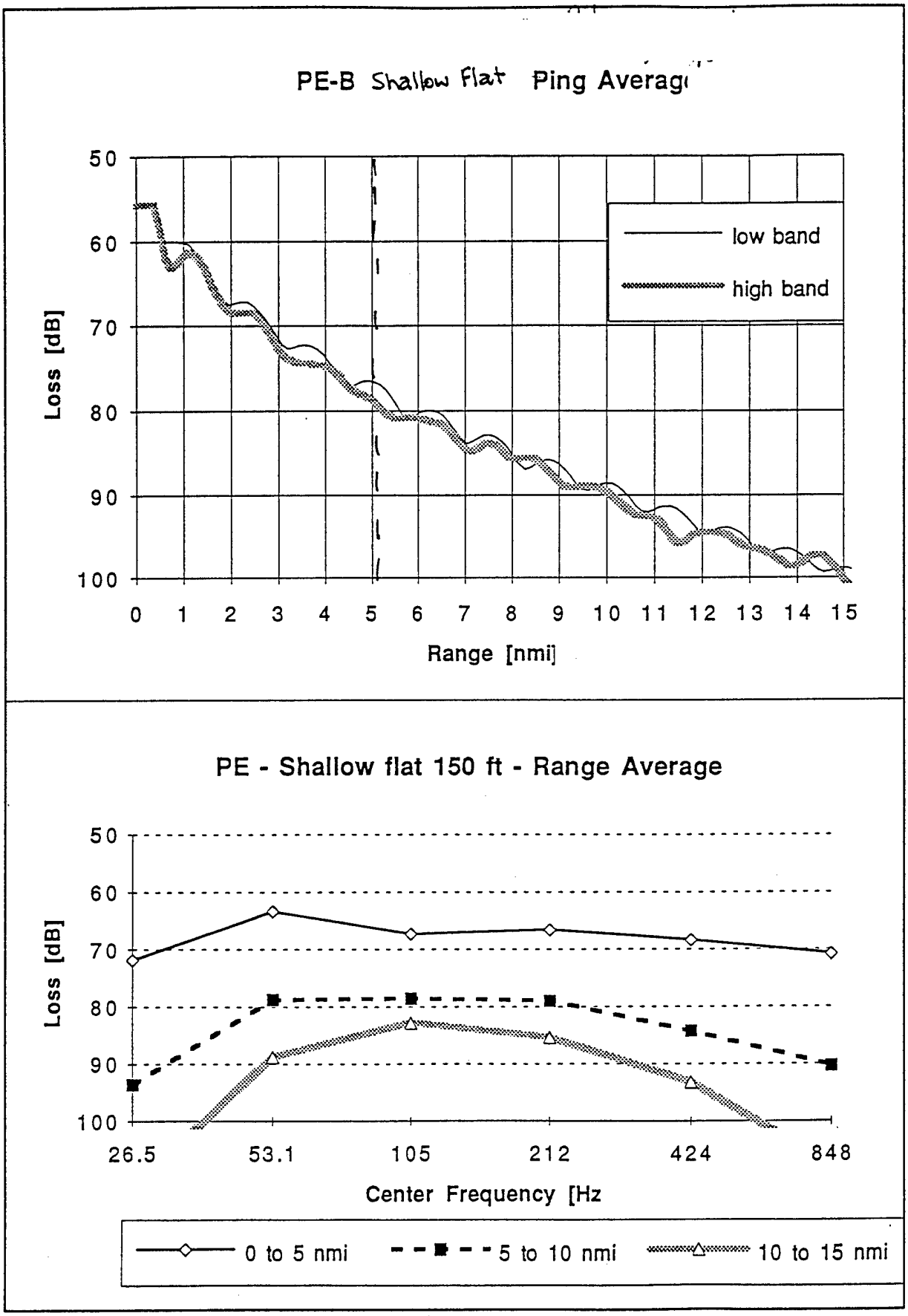
PE-B Shallow Flat Ping Averag
Loss [dB]
50
60
70
80
90
100
0 1 2 3 4 5 6 7 8 9 10 11 12 13 14 15
Range [nmi]
low band
high band
PE - Shallow flat 150 ft - Range Average
Loss [dB]
50
60
70
80
90
100
26.5
53.1
105
212
424
848
Center Frequency [Hz
0 to 5 nmi
5 to 10 nmi
10 to 15 nmi

Figure B-3

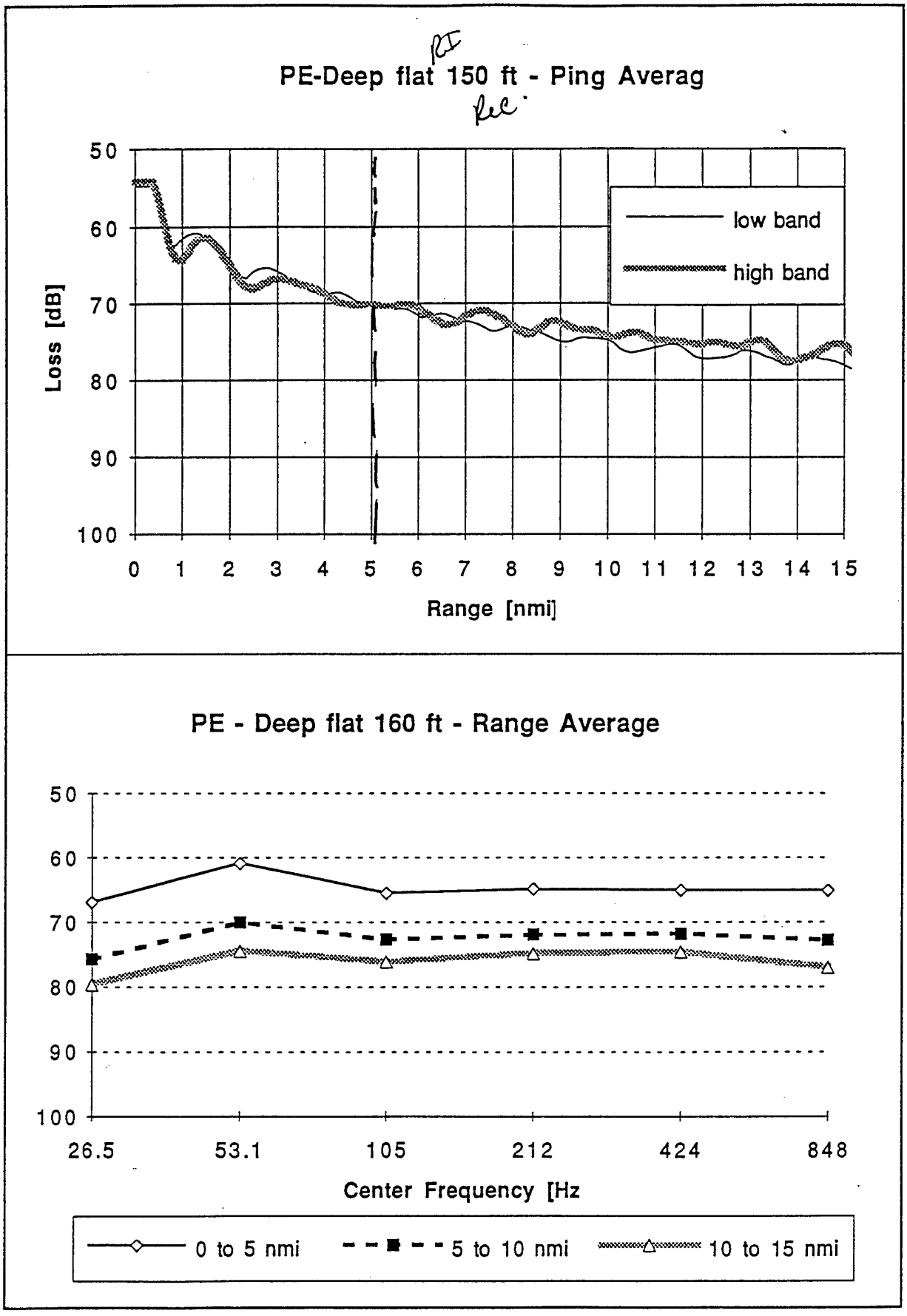
PE-Deep flat 150 ft - Ping Averag
Loss [dB]
50
60
70
80
90
100
0 1 2 3 4 5 6 7 8 9 10 11 12 13 14 15
Range [nmi]
low band
high band
PE - Deep flat 160 ft - Range Average
50
60
70
80
90
100
26.5
53.1
105
212
424
848
Center Frequency [Hz
0 to 5 nmi
5 to 10 nmi
10 to 15 nmi

Figure B-4

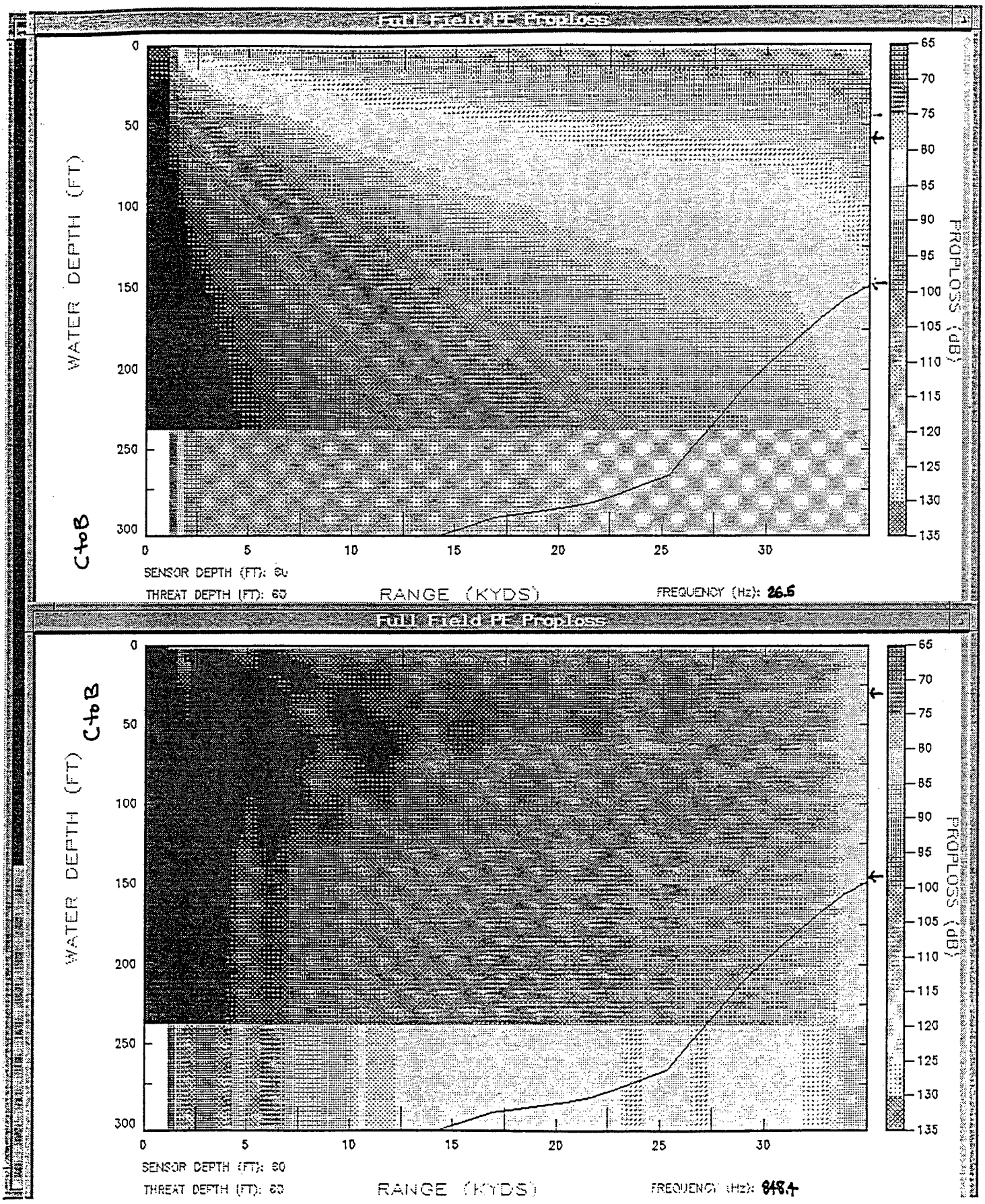
Full Field PE Propioss
WATER DEPTH (FT)
0
50
100
150
200
250
300
0
5
10
15
20
25
30
RANGE (KYDS)
PROPLOSS (dB)
65
70
75
80
85
90
95
100
105
110
115
120
125
130
135
C to B
SENSOR DEPTH (FT): 60
THREAT DEPTH (FT): 60
FREQUENCY (Hz): 26.5
Full Field PE Propioss
WATER DEPTH (FT)
C to B
RANGE (KYDS)
PROPLOSS (dB)
SENSOR DEPTH (FT): 60
THREAT DEPTH (FT): 60
FREQUENCY (Hz): 848.4

Figure B-5

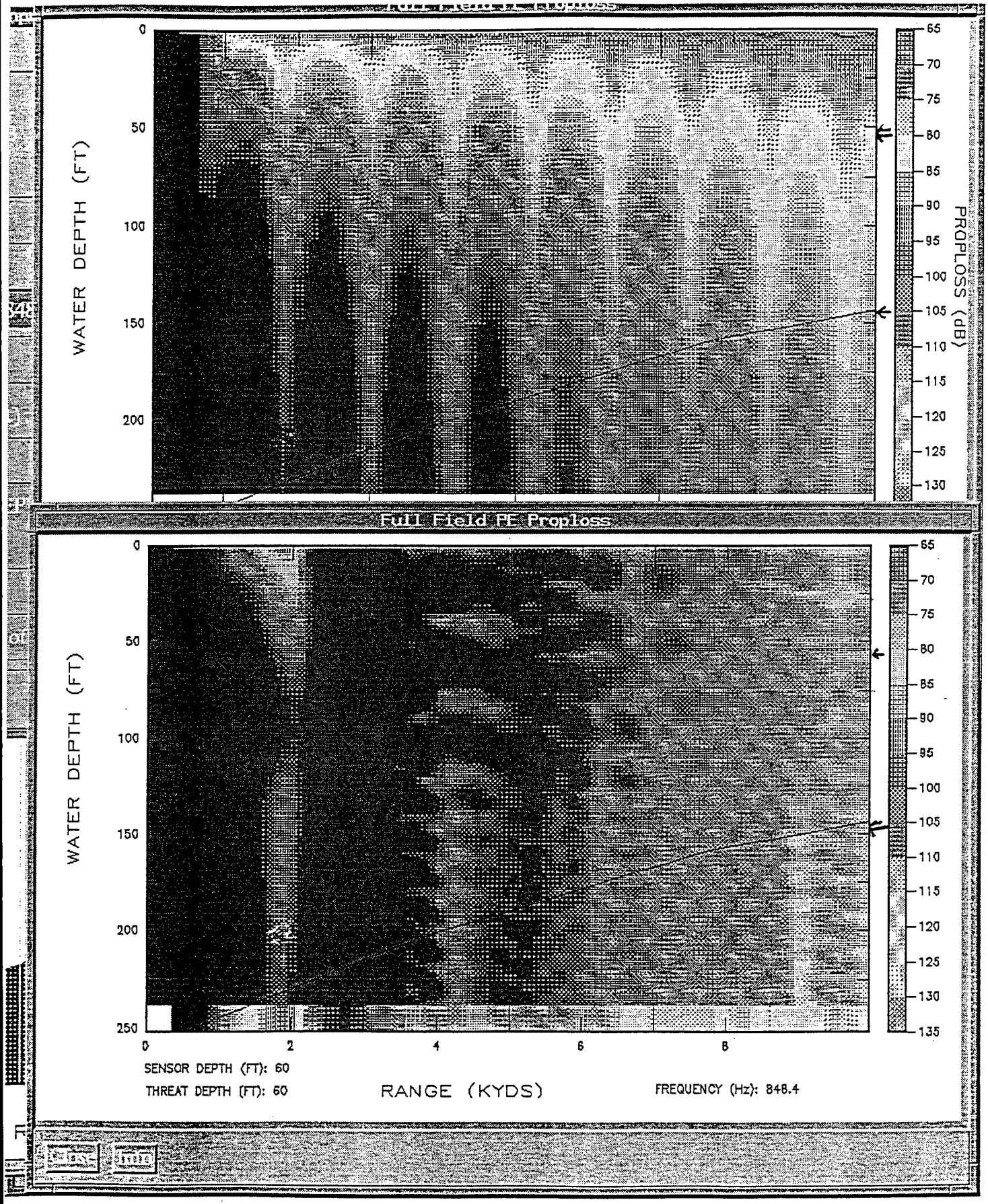
WATER DEPTH (FT)
0
50
100
150
200
PROPLOSS (dB)
65
70
75
80
85
90
95
100
105
110
115
120
125
130
Full Field PE Proploss
WATER DEPTH (FT)
0
50
100
150
200
250
0
2
4
6
8
RANGE (KYDS)
65
70
75
80
85
90
95
100
105
110
115
120
125
130
135
SENSOR DEPTH (FT): 60
THREAT DEPTH (FT): 60
FREQUENCY (Hz): 848.4

Figure B-6

a) BA - CASS - Shallow Receiver

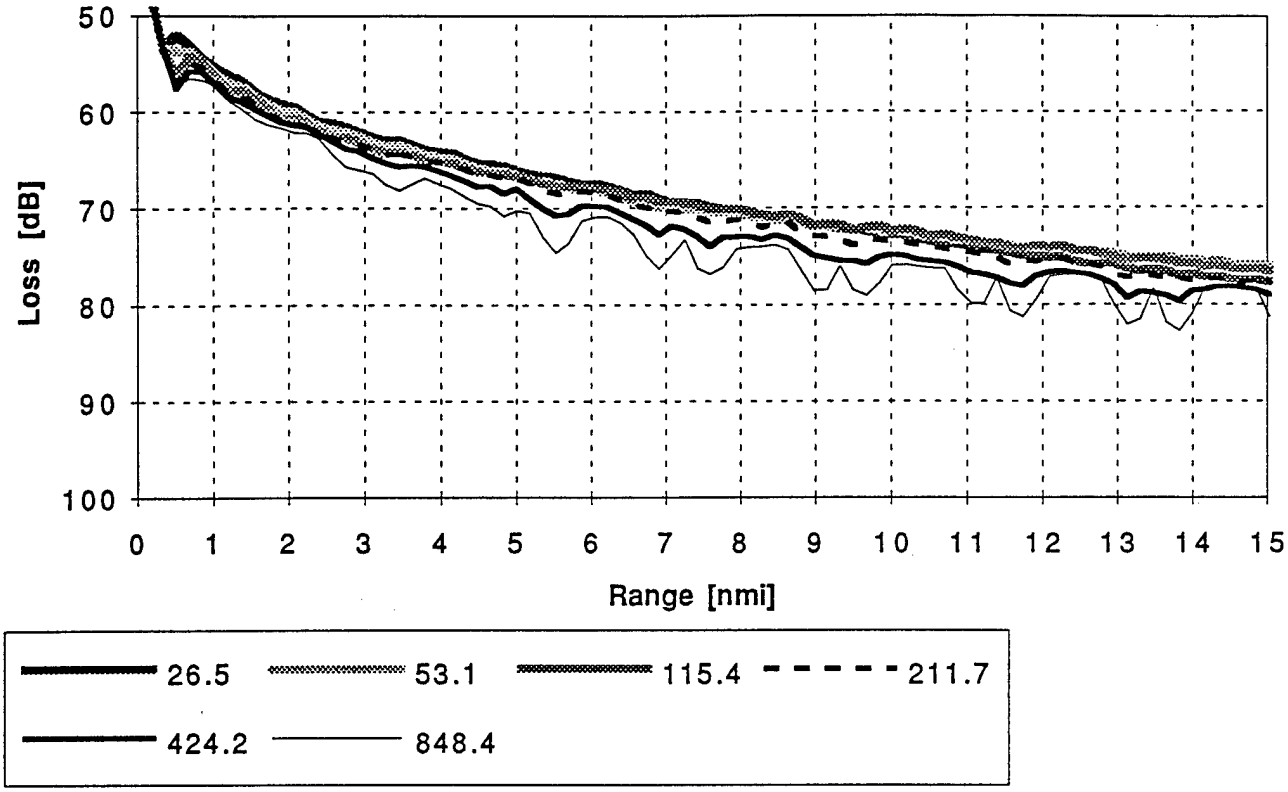

b) Range Avg - BA - CASS - Shallow Receiver

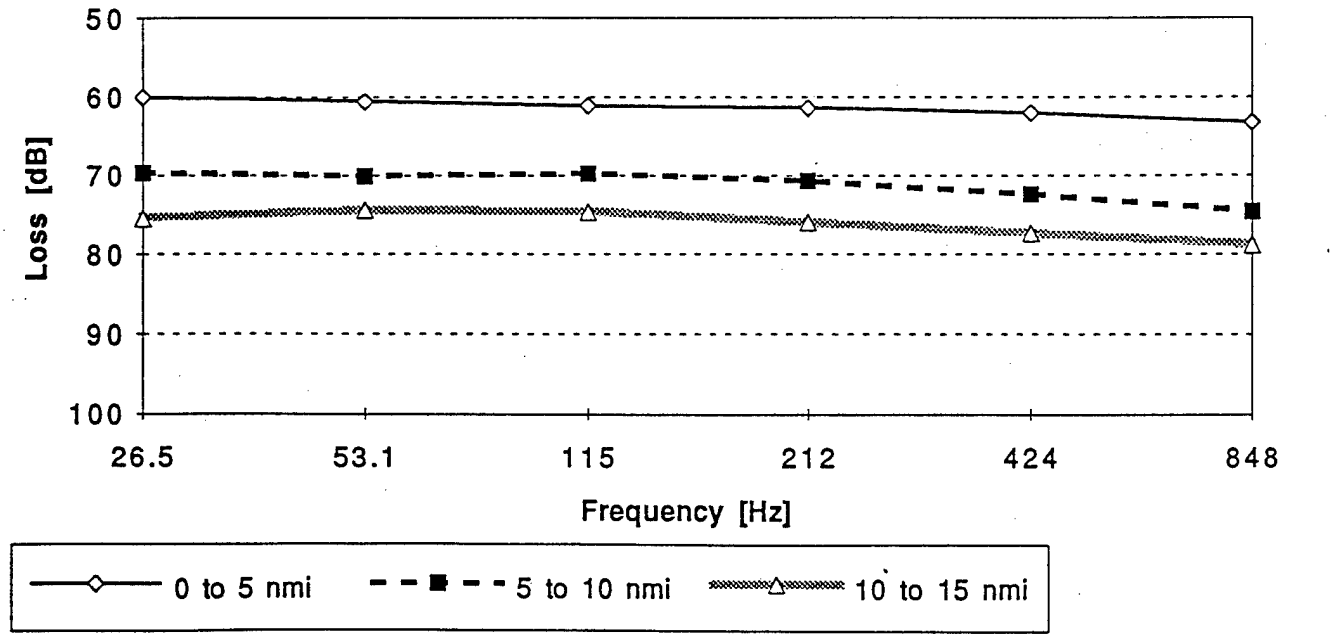

Figure B-7

a) BC - CASS - Shallow Receiver

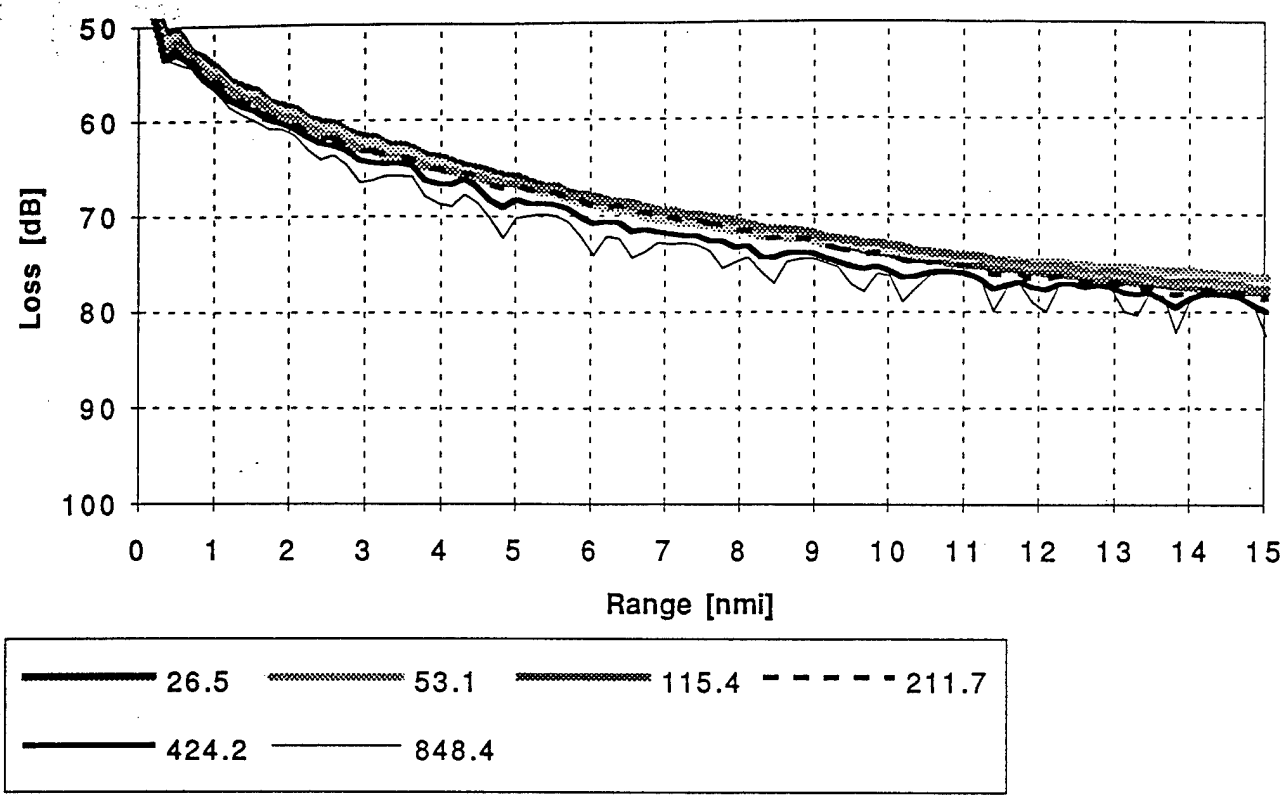

b) Range Avg - BC - CASS - Shallow Receiver

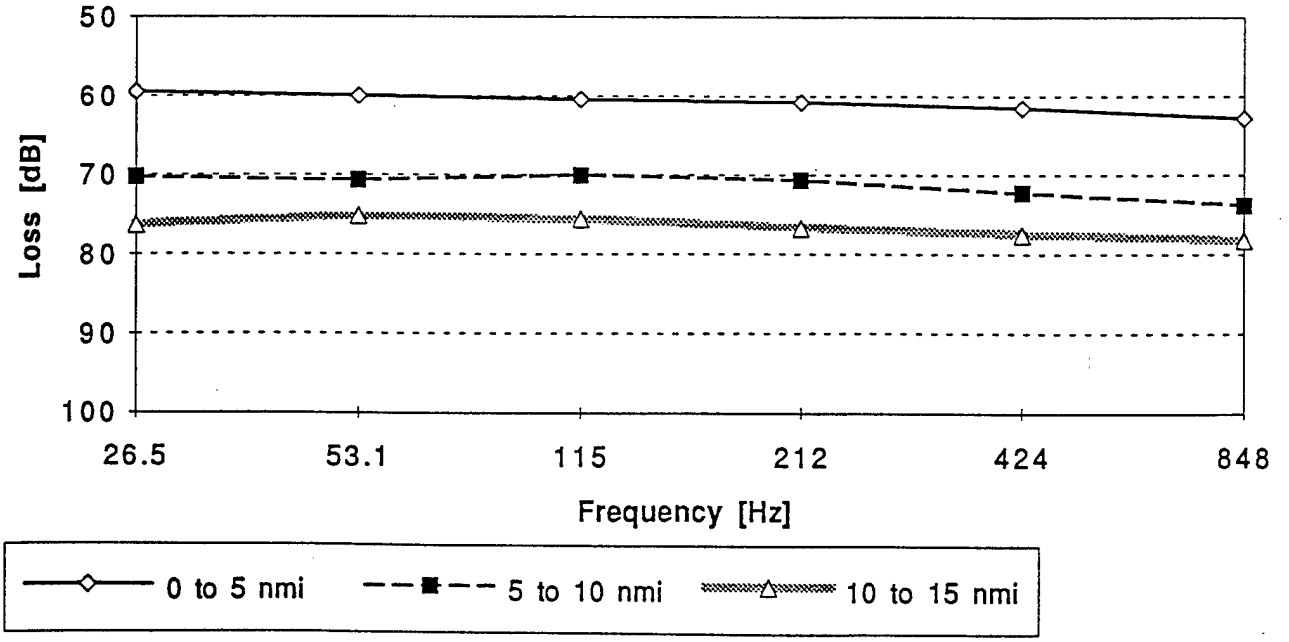

Figure B-8

a) BC - CASS - Deep Receiver

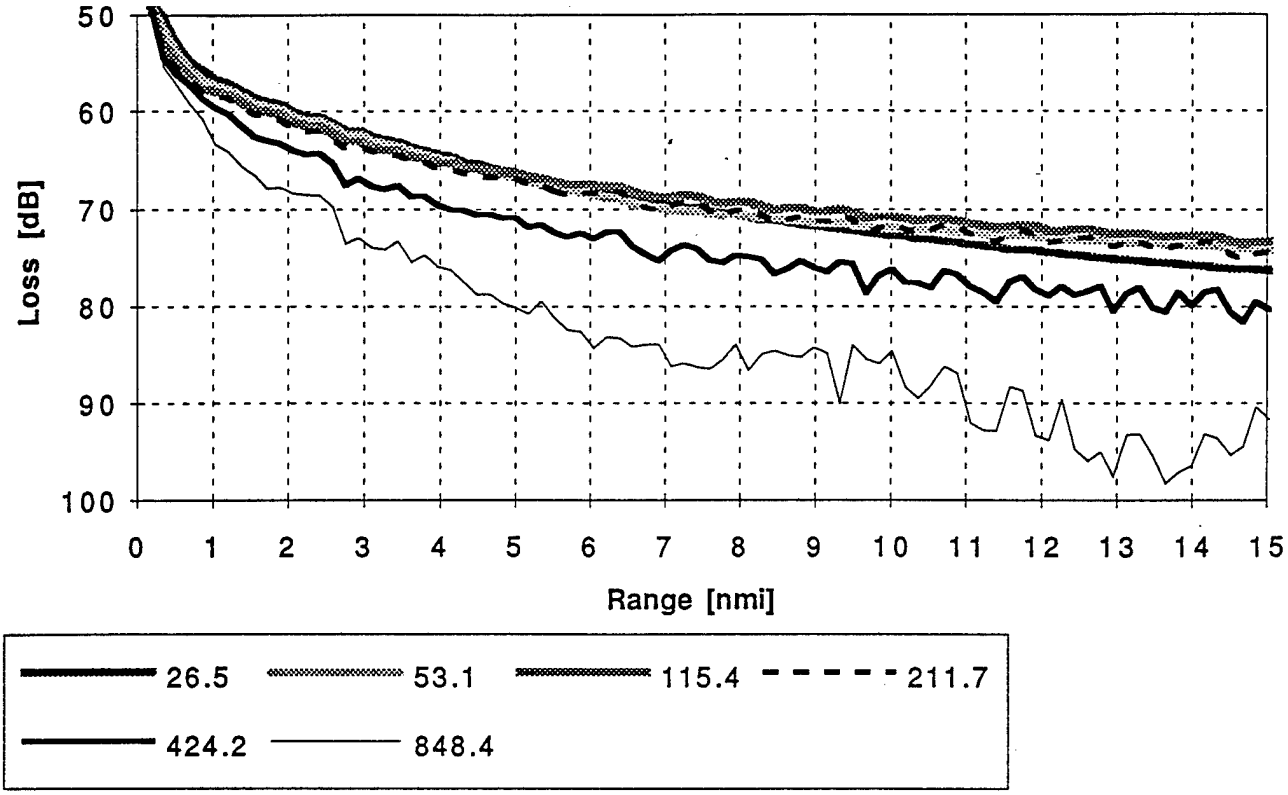

b) Range Avg - BC - CASS - Deep Receiver

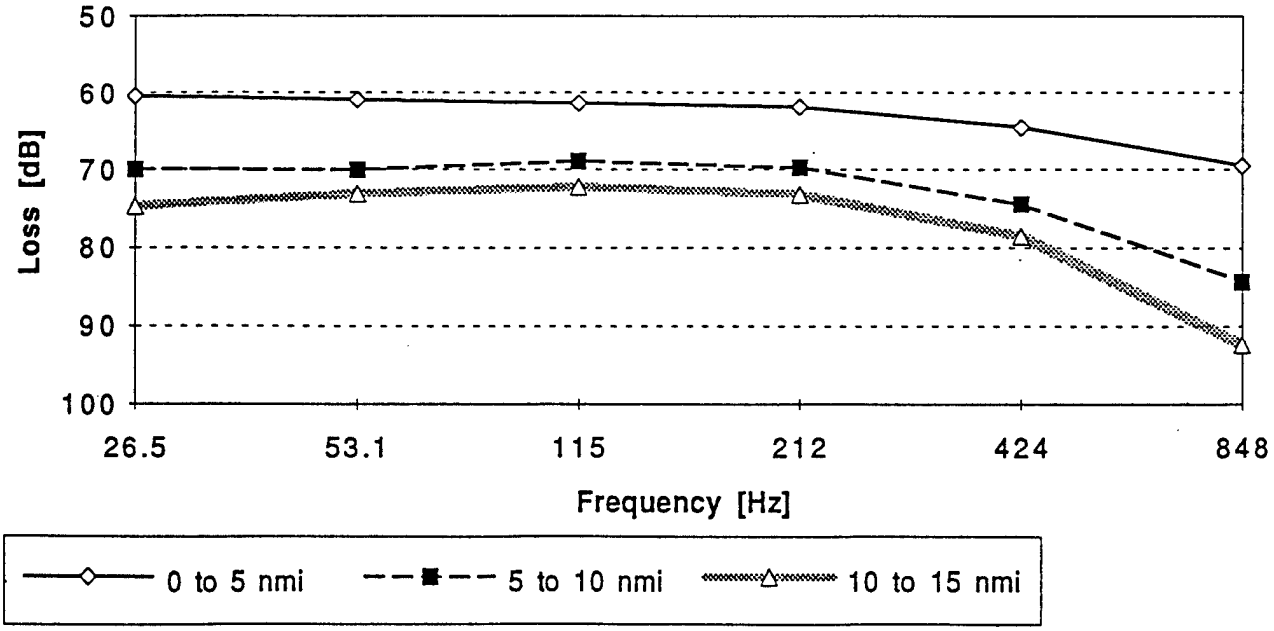

Figure B-9

Appendix C: Full Model Results

The results of the SWAC-1 modeling runs which are used to generate the ping and range averages presented in the text, are given here for reference purposes.

a) BA - PE - Shallow Receiver

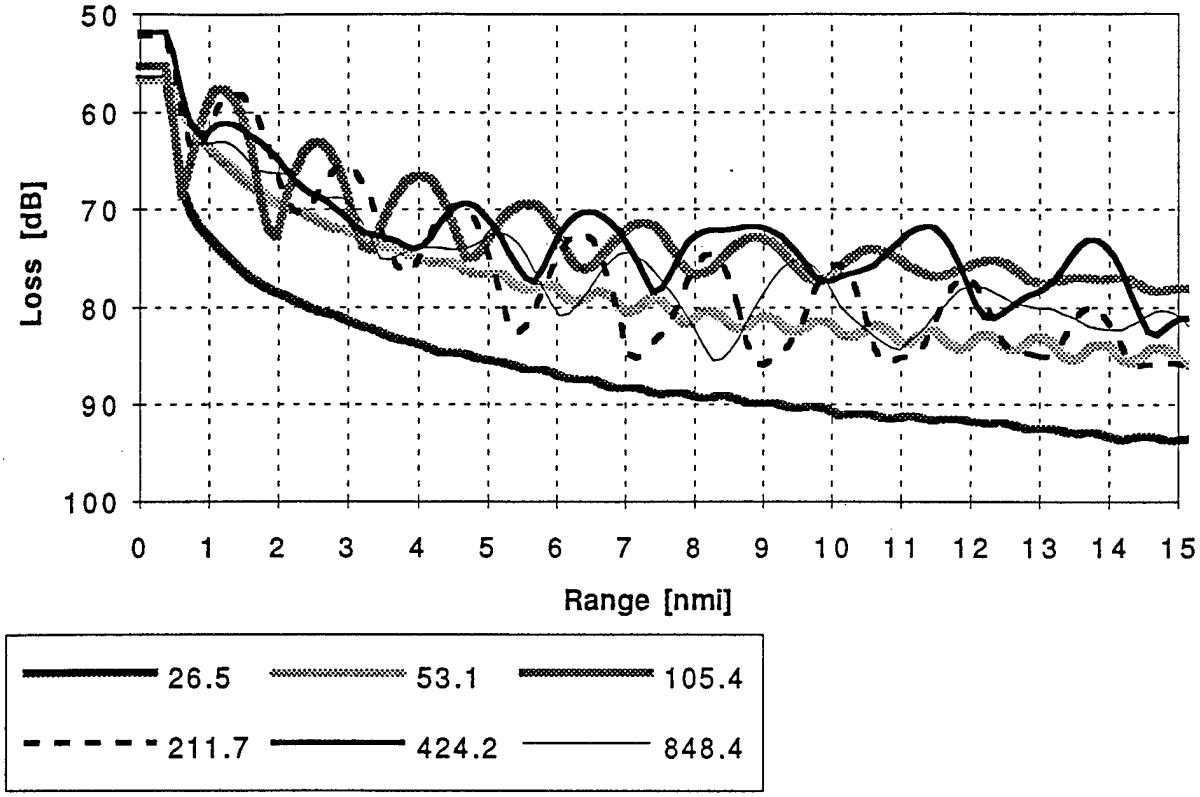

b) Range Average - BA - PE - Shallow Receiver

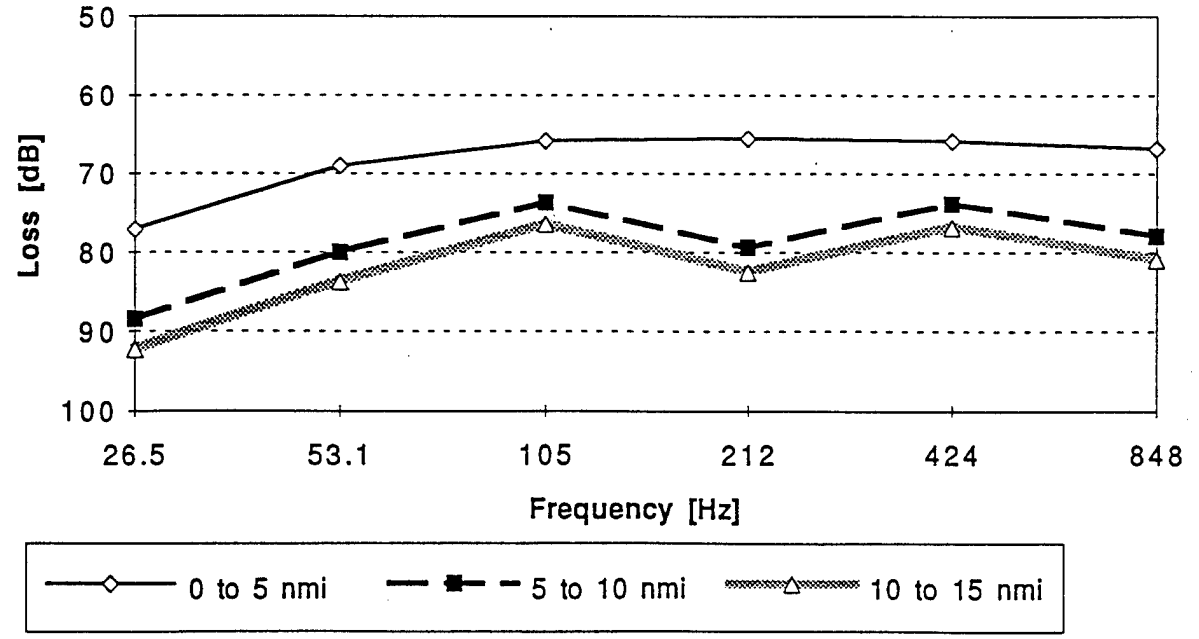

Figure C-1

a) BC - PE - Shallow Receiver

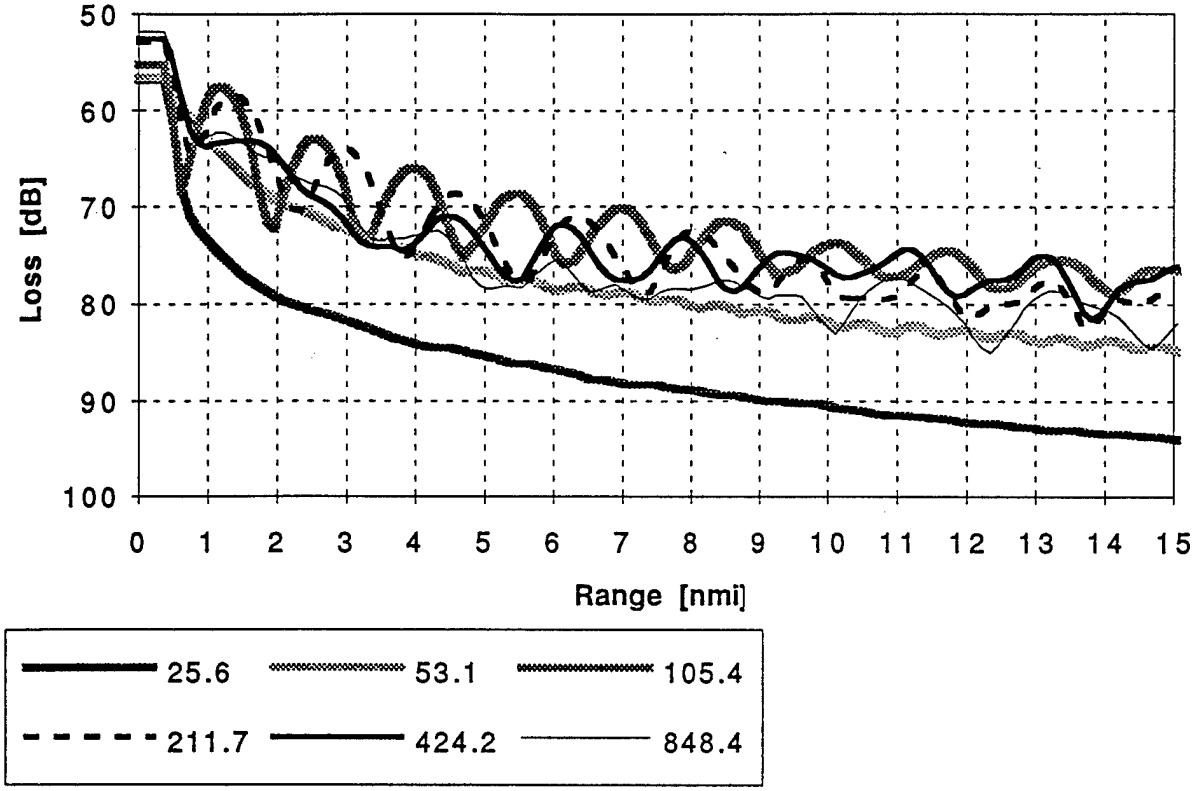

b) Range Average - BA - PE - Shallow Receiver

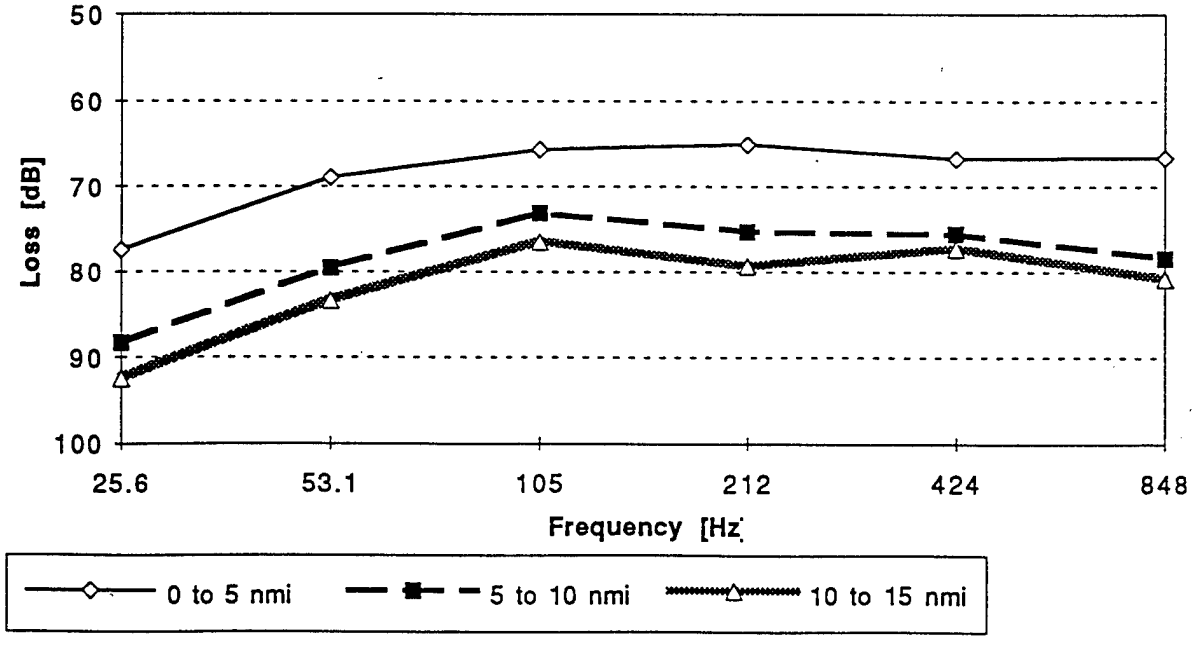

Figure C-2

a) BC - PE - Deep Receiver

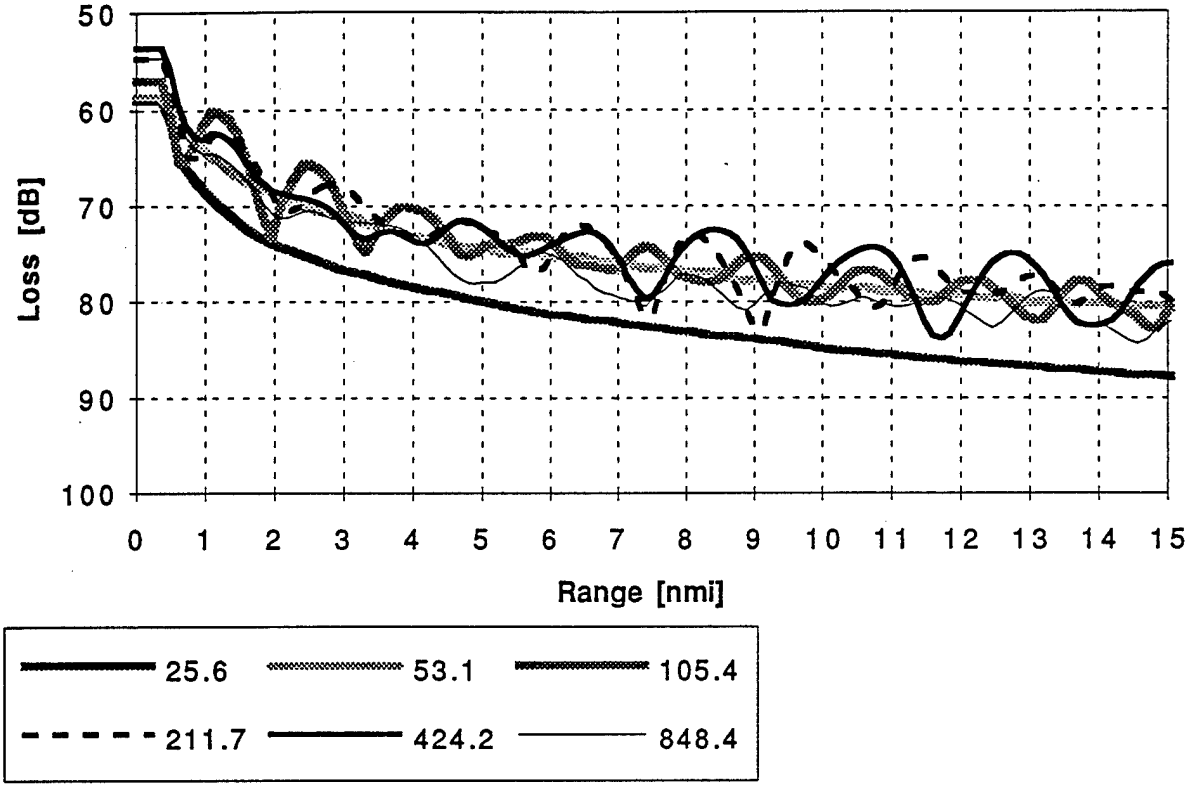

b) Range Average - BC - PE - Deep Receiver

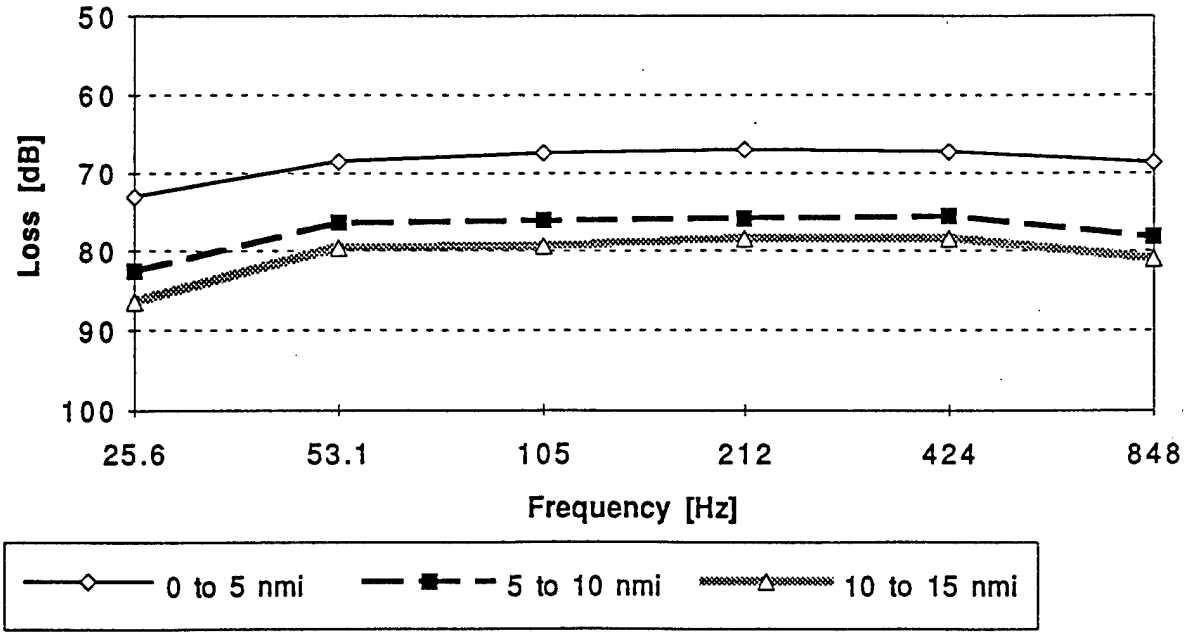

Figure C-3

a) BA - ASTRAL - Shallow Receiver

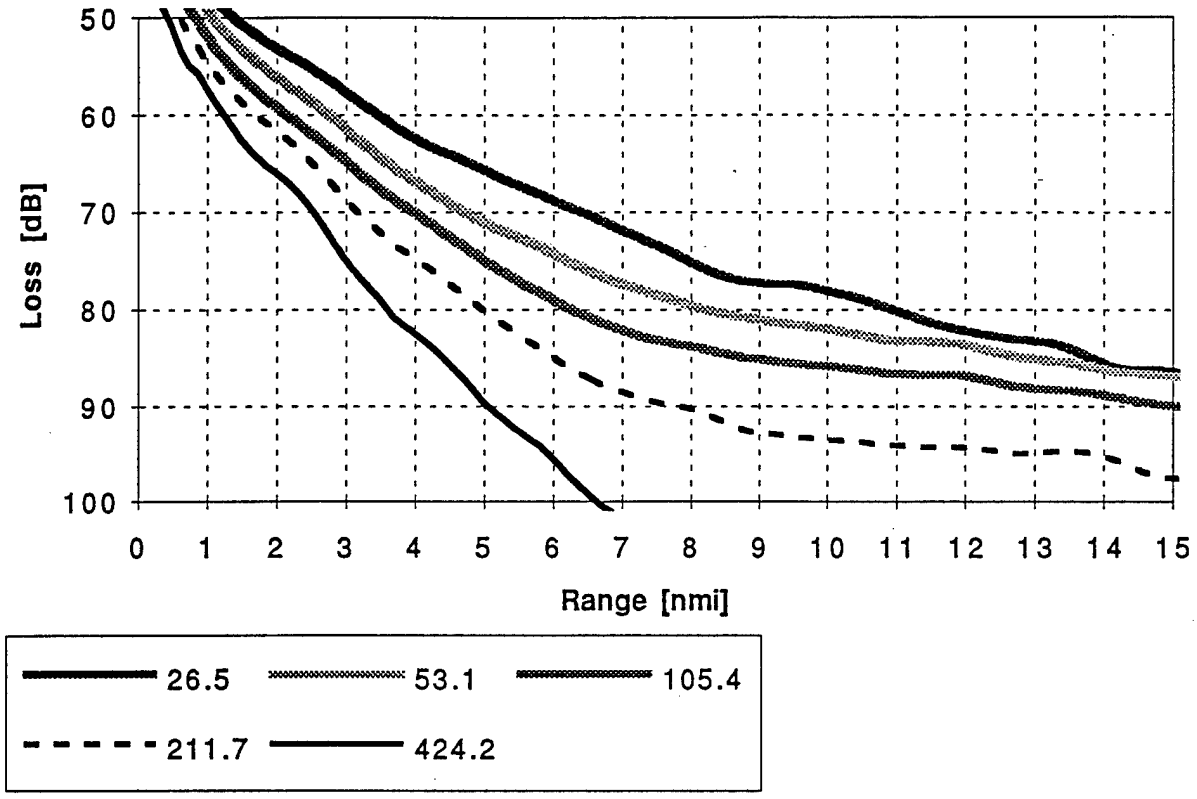

b) Range Avg - BA - ASTRAL - Shallow Receiver

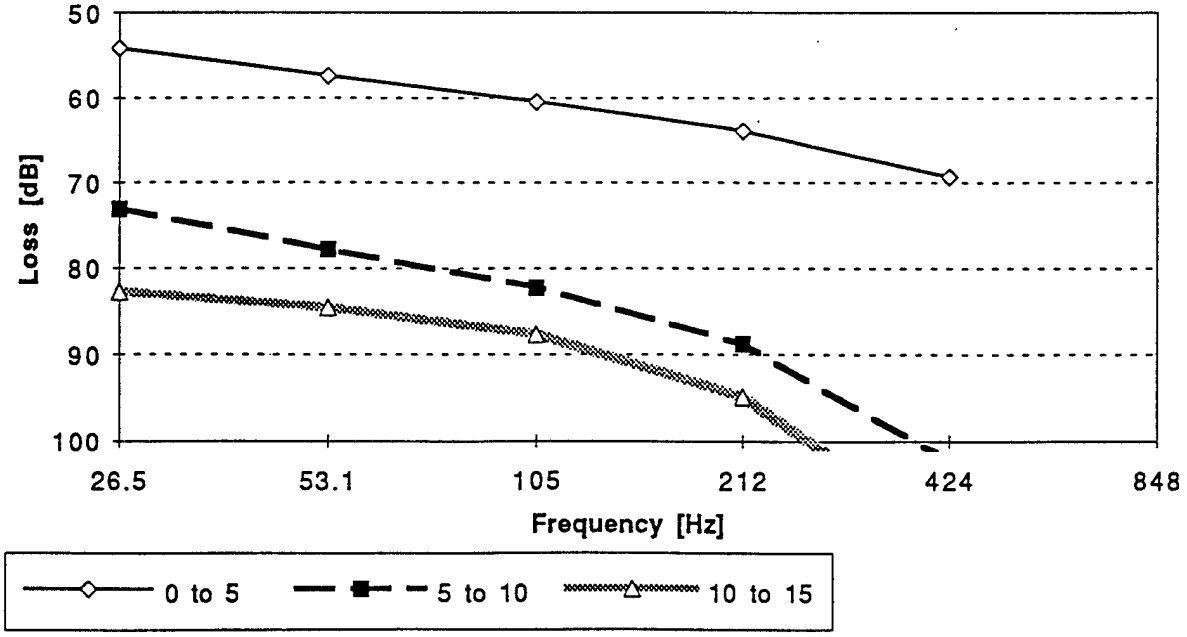

Figure C-4

a) BC - ASTRAL - Shallow Receiver

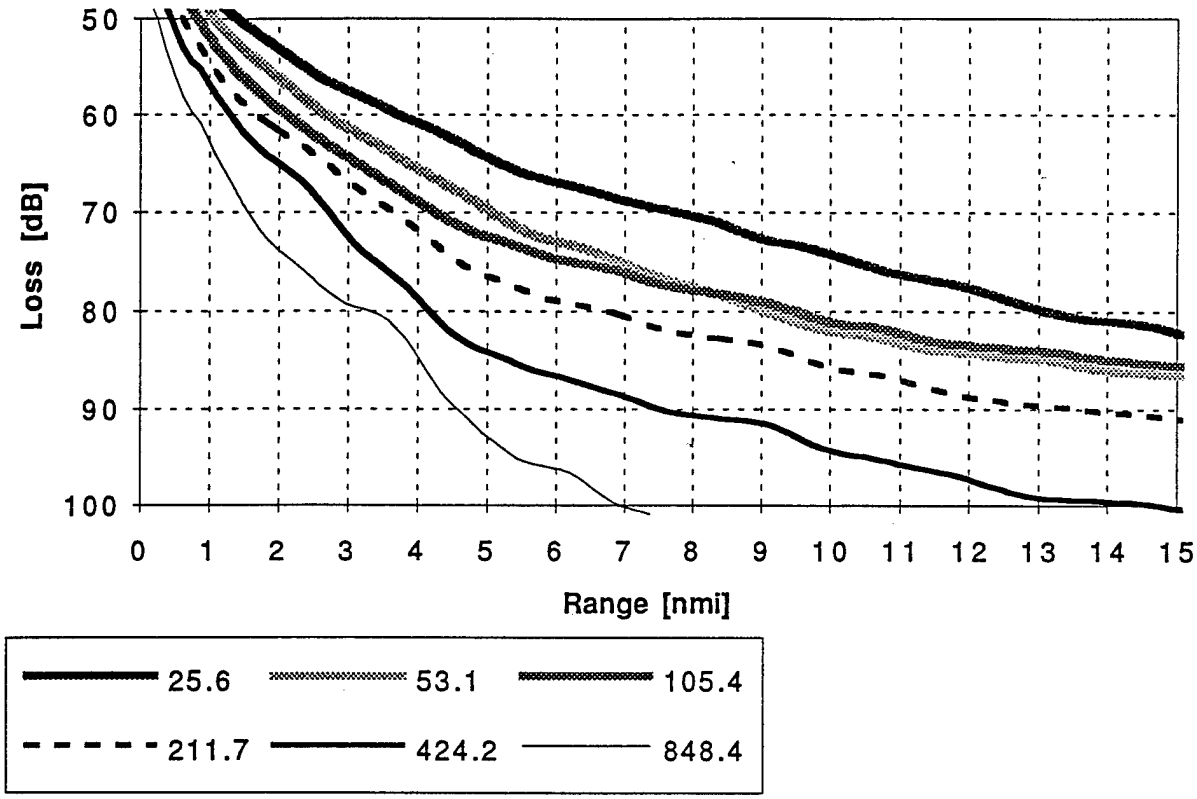

b) Range Avg - BC - ASTRAL - Shallow Receiver

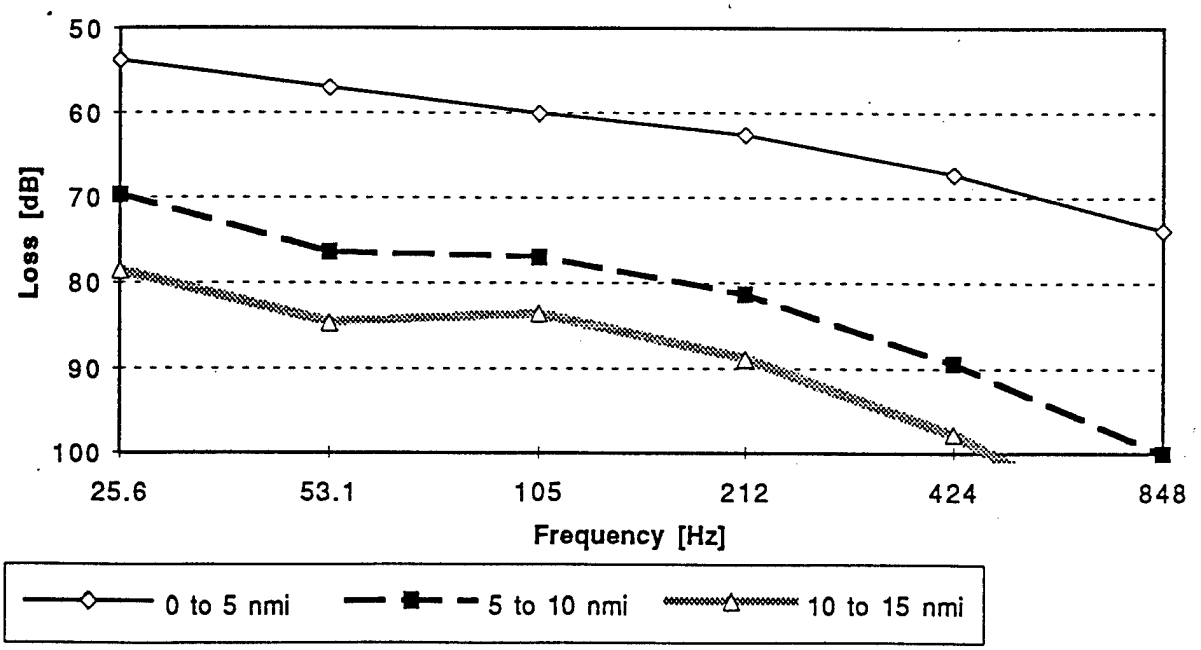

Figure C-5

a) BA - ASTRAL - Deep Receiver

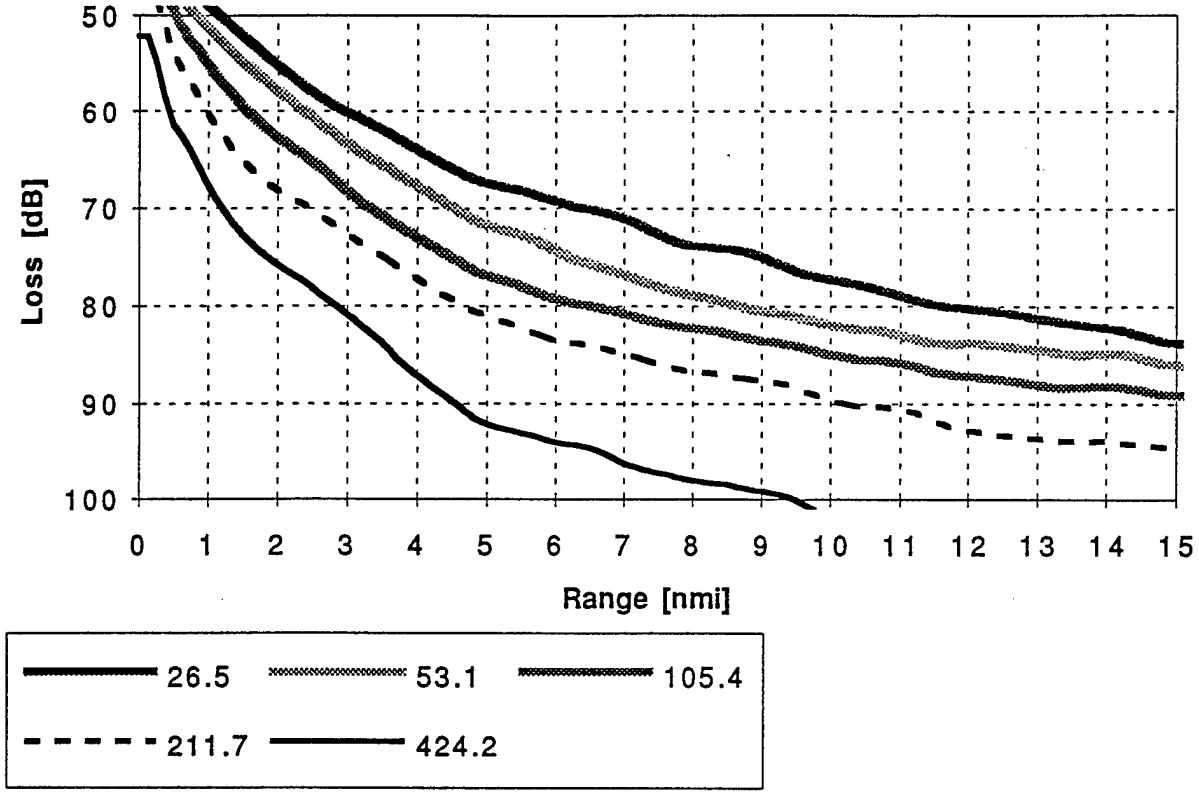

b) Range Avg - BC - ASTRAL - Deep Receiver

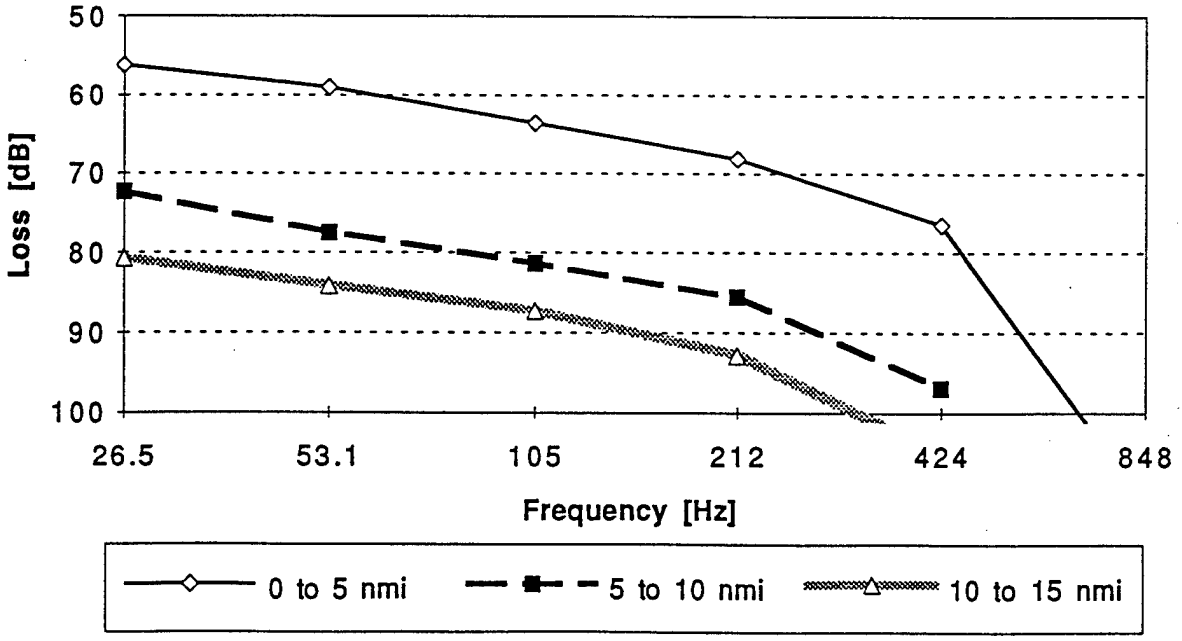

Figure C-6

a) BA - CASS,RFL - Shallow Receiver

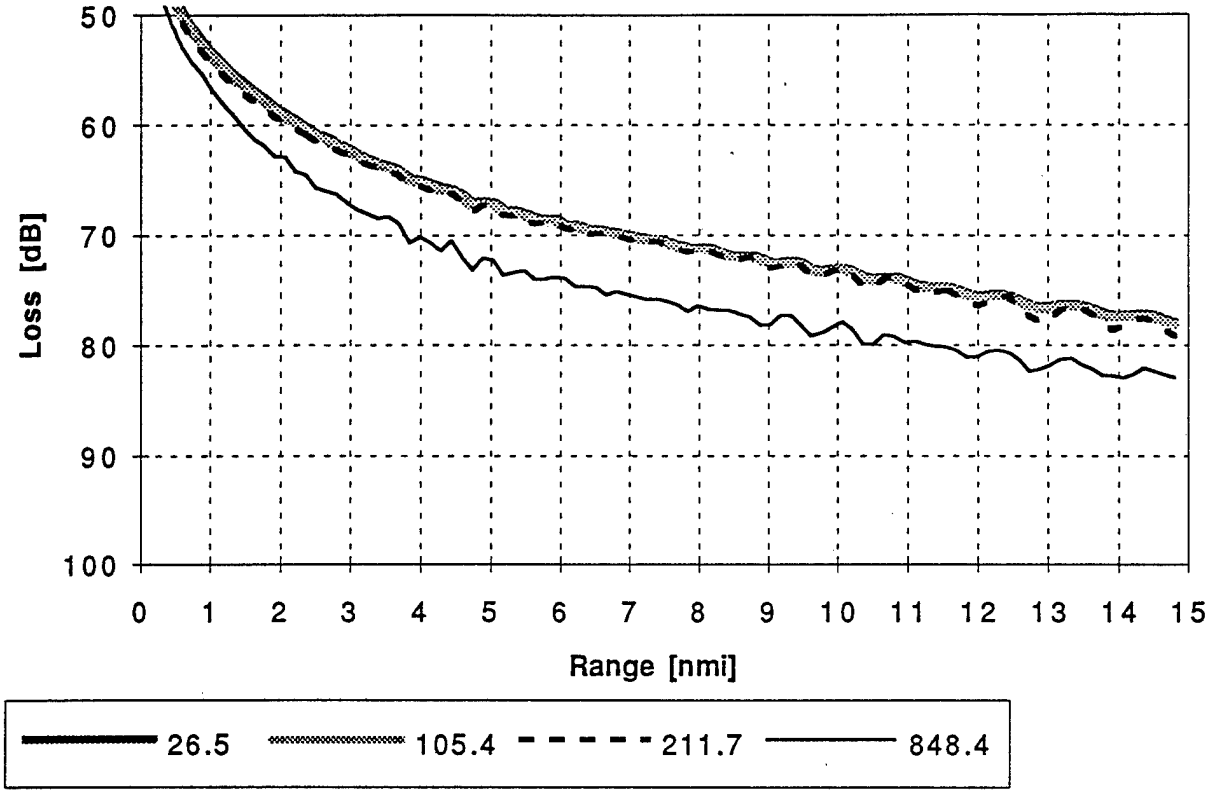

b) Range Avg - BA - CASS - Shallow Receiver

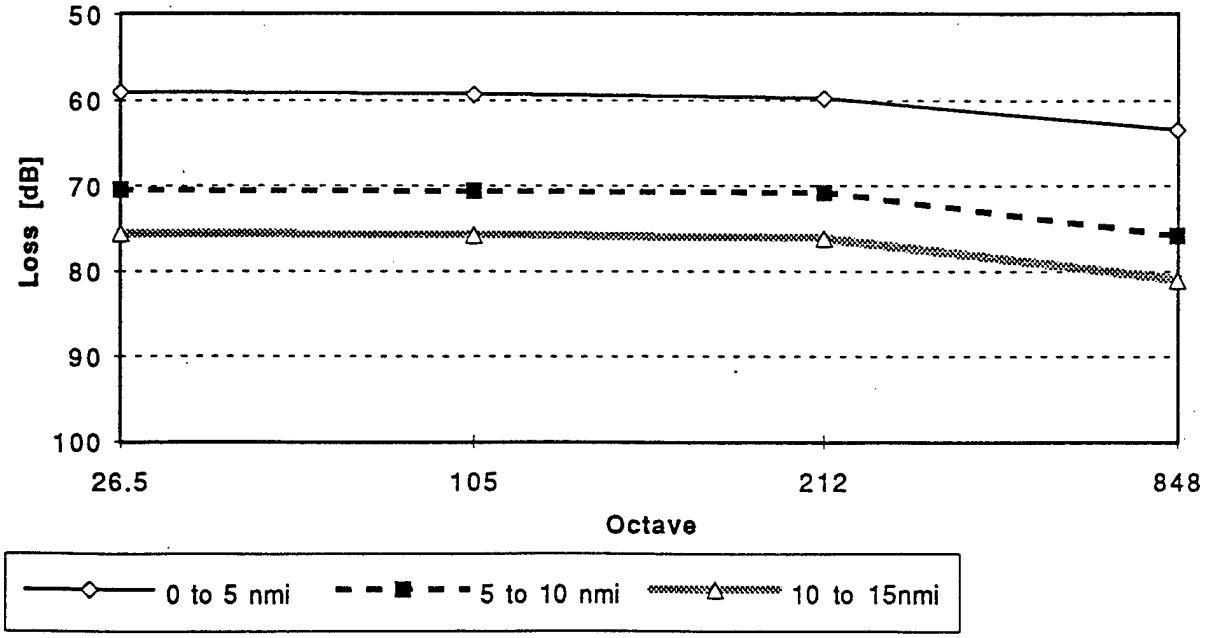

Figure C-7

a) BC - CASS,RFL - Shallow Receiver

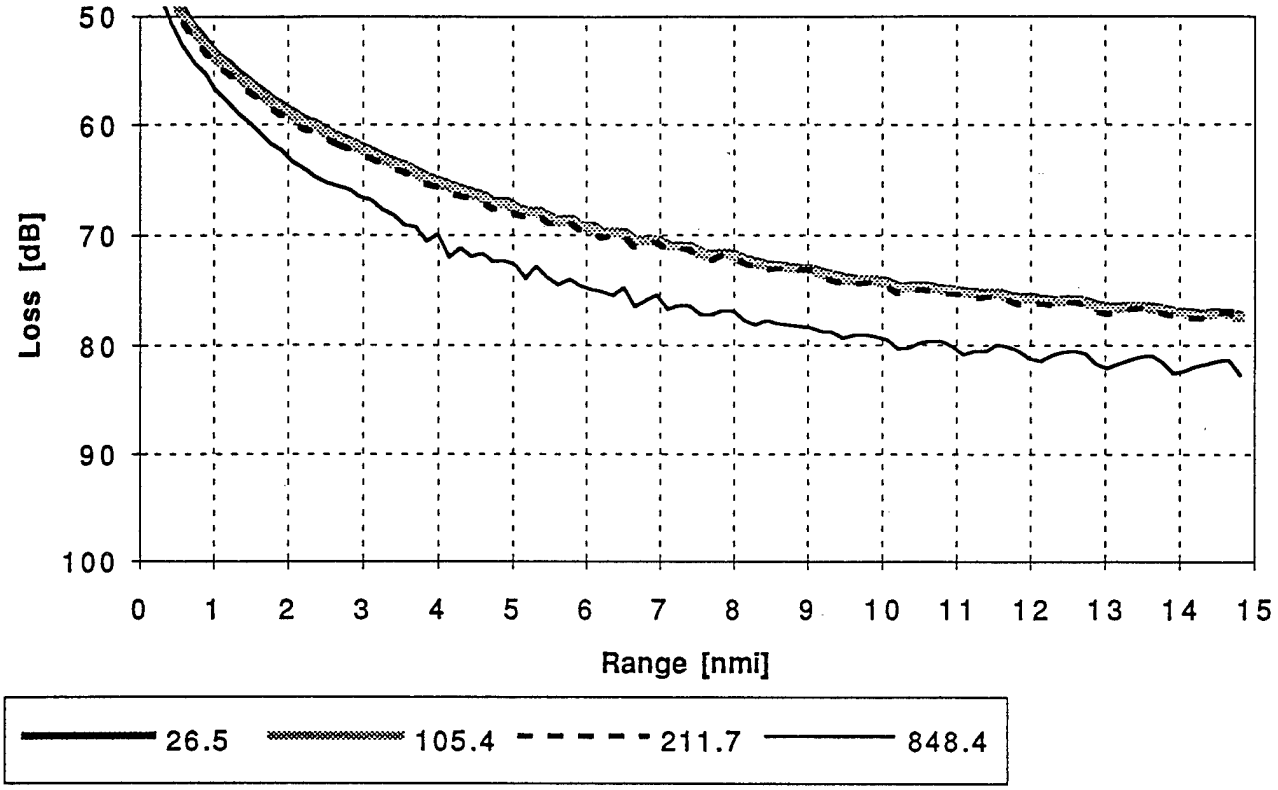

b) Range Avg - BC - CASS,RFL - Shallow Receiver

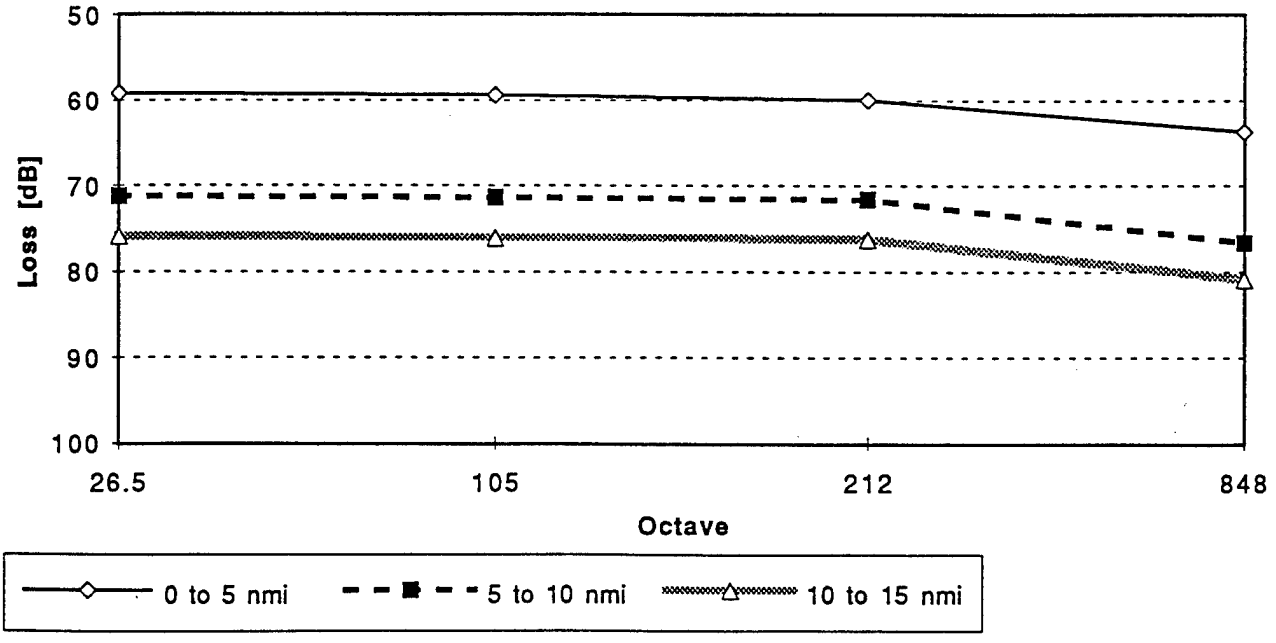

Figure C-8

a) BC - CASS,RFL - Deep Receiver

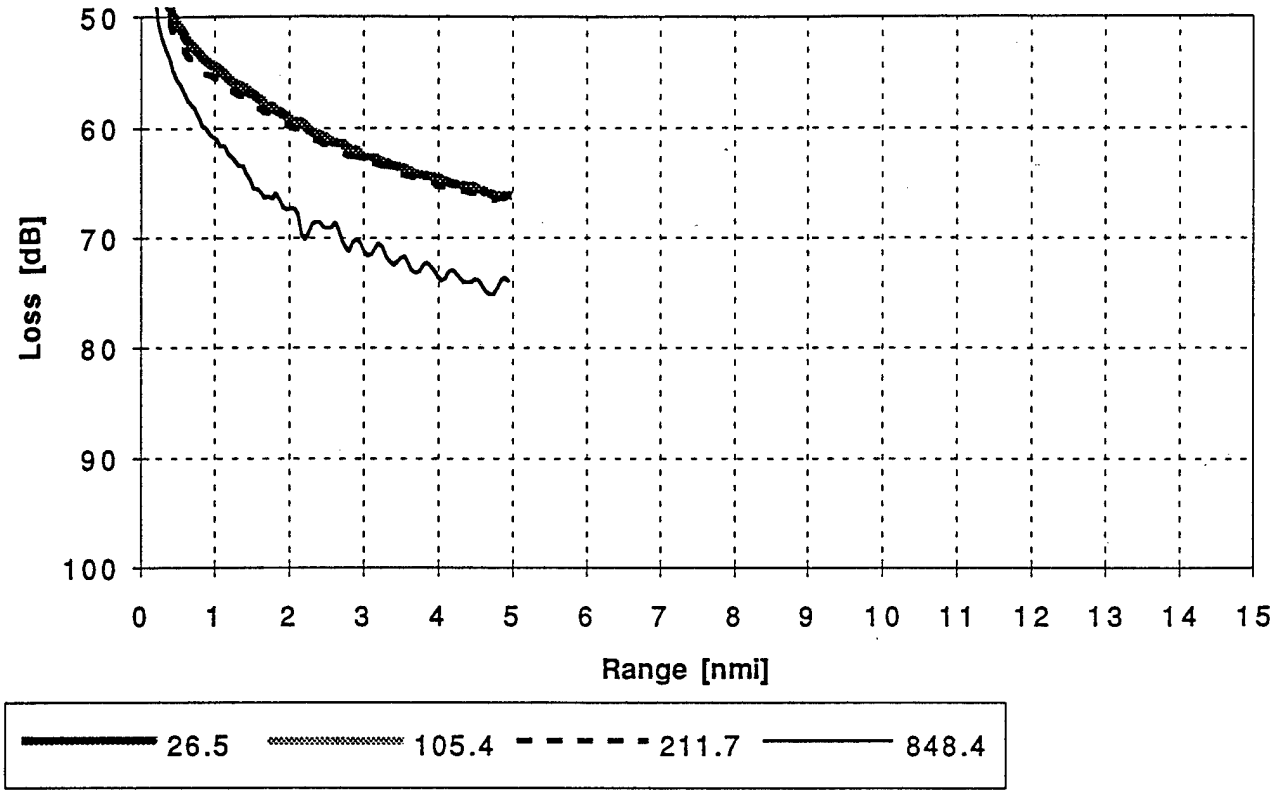

b) Range Avg - BA - CASS - Shallow Receiver

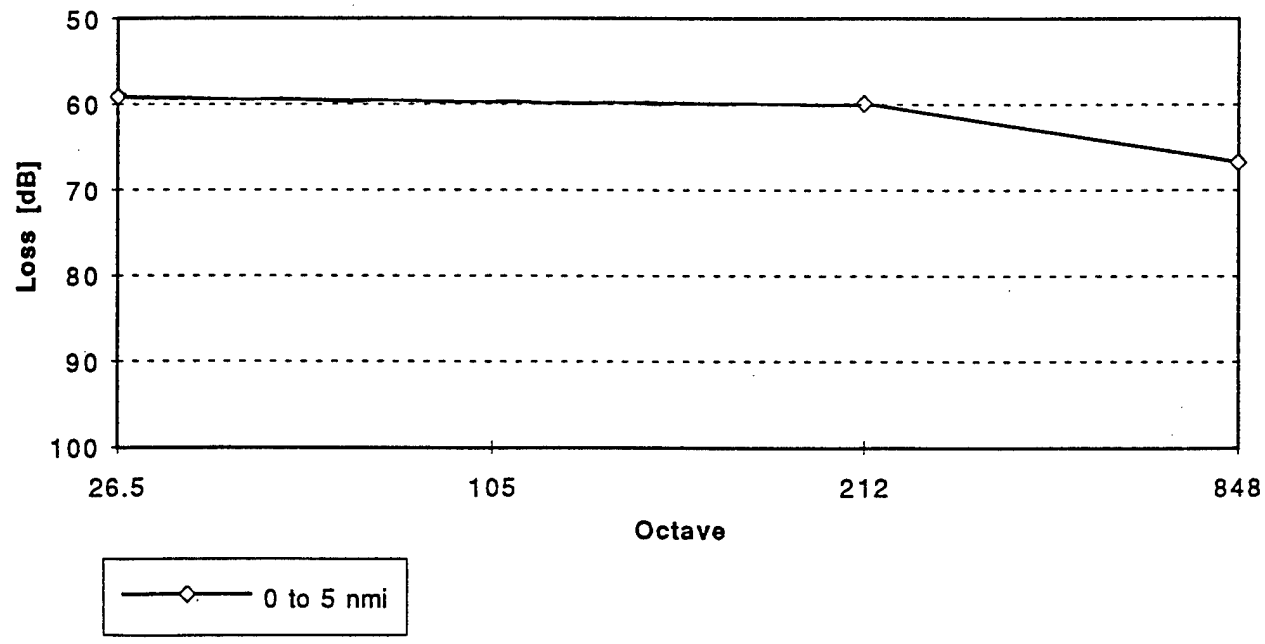

Figure C-9